2006

Design And Implementation Of An Emission Spectroscopy Diagnostic In A High-pressure Strand Burner For The Study Of Solid Propell

Jason Arvanetes
University of Central Florida

DESIGN AND IMPLEMENTATION OF AN EMISSION SPECTROSCOPY DIAGNOSTIC IN A HIGH-PRESSURE STRAND BURNER FOR THE STUDY OF SOLID PROPELLANT COMBUSTION

by

JASON CHRISTOPHER ARVANETES
B.S. University of Central Florida, 2004

A thesis submitted in partial fulfillment of the requirements
for the degree of Master of Science
in the Department of Mechanical, Materials, and Aerospace Engineering
in the College of Engineering and Computer Science
at the University of Central Florida
Orlando, Florida

Spring Term
2006

ABSTRACT

The application of emission spectroscopy to monitor combustion products of solid rocket propellant combustion can potentially yield valuable data about reactions occurring within the volatile environment of a strand burner. This information can be applied in the solid rocket propellant industry. The current study details the implementation of a compact spectrometer and fiber optic cable to investigate the visible emission generated from three variations of solid propellants. The grating was blazed for a wavelength range from 200 to 800 nm, and the spectrometer system provides time resolutions on the order of 1 millisecond. One propellant formula contained a fine aluminum powder, acting as a fuel, mixed with ammonium perchlorate (AP), an oxidizer. The powders were held together with Hydroxyl-Terminated-Polybutadiene (HTPB), a hydrocarbon polymer that is solidified using a curative after all components are homogeneously mixed. The other two propellants did not contain aluminum, but rather relied on the HTPB as a fuel source. The propellants without aluminum differed in that one contained a bimodal mix of AP. Utilizing smaller particle sizes within solid propellants yields greater surface area contact between oxidizer and fuel, which ultimately promotes faster burning.

Each propellant was combusted in a controlled, non-reactive environment at a range of pressures between 250 and 2000 psi. The data allow for accurate burning rate calculations as well as an opportunity to analyze the combustion region through the emission spectroscopy diagnostic. It is shown that the new diagnostic identifies the differences between the aluminized and non-aluminized propellants through the appearance of aluminum oxide emission bands. Anomalies during a burn are also verified through the optical emission spectral data collected.

ACKNOWLEDGMENTS

I would like to acknowledge and thank Siemens Westinghouse Power Corporation (Orlando, FL) for donating the spectrometer used in this experiment. I would also like to thank both The Space Launch Corporation and the Missile Defense Agency MSTARS grant for partial funding of this research effort.

In addition, this work could not have been completed without the hard work of my coworkers, specifically, Rodolphe (Gino) Carro, Alex LePage, Andreiev (Andy) Powell, Tom Sammet, and Matt Stephens.

TABLE OF CONTENTS

LIST OF FIGURES

LIST OF TABLES

LIST OF ACRONYMS/ABBREVIATIONS

AP	Ammonium Perchlorate
Al	Aluminum
CCD	Charge Coupled Device
DAQ	Data Acquisition
GUI	Graphical User Interface
HTPB	Hydroxyl-Terminated-Polybutadiene
IPDI	Isophorone Diisocyanate
MDI	Diphenyl Methane Diisocyanate
ND	Neutral Density
PC	Personal Computer
S/N	Signal-to-Noise
UCF	The University of Central Florida
USB	Universal Serial Bus

CHAPTER ONE: INTRODUCTION

Solid rocket propellants have traditionally been used in high-thrust applications such as boosters for launching space vehicles or as propulsion systems for tactical weapons where a compact size is necessary. Composite solid propellants are commonly utilized in rockets because of their high burn rates and favorable specific impulse (Davenas, 2003). The chemistry of a typical composite propellant consists of three (3) main ingredients: fuel, oxidizer and, binder. HTPB/AP-based propellants continue to be of interest, and modifying the burn rate of this propellant combination continues to be an area of active research. Under burning conditions, the fuel and oxidizer react creating hot, gaseous combustion products. The gases form within a combustion chamber and escape through a converging-diverging nozzle, thus thrust can be produced. Many of the fundamental processes that occur during solid propellant combustion are still unknown, and the development of new propellants remains highly experimental (Sutton and Biblarz, 2001; Davenas, 2003).

In solid propellants, powdered metals, primarily aluminum, have been in use for over four decades because of their potential for high flame temperatures and increased performance. However, problems with melting temperatures, residence times, and oxide coatings often prevent the high potential of metal powders from being fully realized (Bukaemskii, 2002; Price and Sigman, 2000). The physical mechanisms controlling the heating, vaporization, and combustion of aluminized solid propellant ingredients are challenging and continue to be the subject of active research both theoretically and numerically (Sambamurthi et al., 1984; Fitzgerald and Brewster, 2004).

Potential areas where performance enhancement and burn rate tailoring can be made include additives, smaller solid particle sizes, and various metallic fuel combinations (Brill and Budenz, 2000; Dokhan et al., 2002b). Recent research at The University of Central Florida has investigated particle size dependencies and the effects of additives (Small et al., 2005; Stephens et al., 2005a; Stephens et al., 2005b). The intent of this newer research is to gain a better understanding of the complex combustion process. Through this new knowledge, the chemistry can more effectively be modified to produce a better, more efficient propellant or a propellant tailored for a very specific or unique purpose.

While critical burn rate information is obtained from the strand burner setup, additional knowledge of the details of the burning process is useful in determining the fundamental behavior of the propellant mixtures with and without the additives. Because of the harsh, high-pressure environment of the strand burner, detailed measurements using intrusive means are difficult. The focus of the present study is therefore on the incorporation of an emission spectroscopy diagnostic onto the high-pressure strand burner experiments. To better identify the reactions occurring within the laboratory, a spectrometer was added to the testing apparatus (Arvanetes and Petersen, 2006). The data gleaned from the spectrometer identify the predominant gaseous species present during reaction.

Since the time scale of the burn is on the order of one second for typical solid propellant strand samples, there is plenty of time within the limits of the spectrometer setup and computer data acquisition system (~ 1 ms combined), allowing for several readings to be taken as a function of time. Others have used similar emission techniques to study the burning of solid propellants and related particles, such as Glumac et al. (Glumac et al., 2005).

There are various reasons for adding the spectrometer diagnostic capability to the existing strand burner facility, namely: 1) to determine if certain additives are participating chemically in the combustion process or whether they are acting as a type of catalyst by looking for the emission from their gas-phase intermediates; 2) to verify the baseline combustion behavior of both metallized and non-metallized propellants from test to test; 3) to watch for any correlation between the emission signature during a typical burn and incomplete combustion, explosions due to voids, and other anomalous behavior; and 4) to infer gross temperatures and relative concentrations.

Provided in this thesis is a discussion on solid propellants and emission spectroscopy followed by an explanation of the research and an analysis of the data collected. The research involves the addition of a compact spectrometer to a strand burner facility for testing solid rocket propellants and analyzes the data collected from both the spectrometer as well as the existing diagnostics.

CHAPTER TWO: BACKGROUND

Rocket Fuel

The basic composition of a typical high burn rate propellant with a high solids loading consists of 10.5% HTPB binder, 20% aluminum powder, 67.5% AP, 0.5% Iron Oxide (Fe_2O_3), and 1.5% MDI curative. A basic non-metallic propellant contains 18.1% HTPB binder, 80% AP, 1.7% IPDI curative, and 0.2% Tepanol. In the non-metallic propellants, the HTPB, a complex, polymer hydrocarbon, acts as the fuel source in the absence of Aluminum.

A common descriptive parameter of solid rocket propellants is the burn rate. As the combustion chamber pressure increases, the propellants burn faster. The empirical correlation between pressure and burn rate follows:

$$r = AP^n$$

Where r is the burn rate, A is a constant, P is the pressure, and n is the pressure exponent. A and *n* are calculated by testing a propellant across a range of pressures and fitting an appropriate exponential curve to the data (Sutton and Biblarz, 2001).

There has been much interest in recent years to better understand the chemical reactions occurring within rocket fuel as well as typical individual components of composite propellants. Apte and Yang have studied the combustion dynamics of solid propellants (Apte and Yang, 2002). The products of propellant combustion have been studied to further determine the reactions during burning (Glotov, 2002). Aluminum particle combustion has attracted many

researchers. For example, the ignition of a single aluminum particle was studied by Federov and Kharlamova taking into consideration the rapid oxide growth (Federov and Kharlamova, 2003).

Through the use of smaller particle size components, the surface area of ingredients in contact with other ingredients increases significantly. Positive benefits of replacing micron-scale powders in solid propellants with nano-sized particles have been demonstrated by researchers such as Dokhan et al. (2001, 2002a, 2002b, 2003), Lessard et al. (2001), Popenko et al. (2002), and Granier and Pantoya (2004). A recent study at The University of Central Florida (UCF) investigated the use of multiple-size particles, or bimodal, Ammonium Perchlorate (AP) and the effect on burn rate (Stephens et al., 2005b). There have been studies on adding non-typical components to a standard composite propellant composition such as Iron Oxide (Fe_2O_3) or Titania (TiO_2) particles (Sutton and Biblarz, 2001). Nano-scale Titania particles were grown and incorporated into an aluminized composite propellant to study their effect on the propellant's burn rate (Small et al., 2005).

Researchers have taken interest in nano-scale aluminum as a means for significantly increasing the burn rate of aluminum-based propellants or the released energy of explosives (Stephens et al., 2005a; Brousseau and Anderson, 2002; Mench et al., 1998; DeLuca et al., 2005). Advantages to using submicron Al particles as some fraction if not all of the fuel are mostly based on their increased surface-to-volume ratio, allowing decreased melting and vaporization times and their increased contact with the propellant oxidizer, usually ammonium perchlorate (AP). Non-aluminized propellants have also been studied. Propellants with low pressure sensitivity tend to be more stable (Chakravarthy et al., 2001). Many questions regarding the application and effects of nano-sized aluminum on the processing, strength, burn rate, and acoustic properties of AP-based composite propellants are still unanswered

(Blomshield, 2004). One problem in particular is the introduction of the fine metal powder into the propellant matrix.

The military's interest in developing high burn rate propellants for tactical use date back into the 1960's and 1970's. In a final report from 1971, Aerojet presents their development work and findings to the Naval Weapons Center at China Lake, California (Lou and Katzakian, 1971).

Hybrid rocket motors typically utilize a gaseous oxidizer such as Oxygen (O_2) or Nitrous Oxide (NO) that is introduced into a combustion chamber through an injector. The combustion chamber is similar to that of a standard rocket propellant in that the combustion products line the walls of the chamber. The solid material inside a hybrid rocket motor is the solid fuel only; the oxidizer is injected and reacted. A major advantage of hybrid rocket motors is the ability to throttle, or control the thrust, of the motor. Like in solid rockets, as the fuel combusts and is exhausted, the volume of combustion chamber increases. This fuel regression rate is used to help identify the available burn time within a rocket motor (George et al., 2001). Subscale hybrid motors containing ultra-fine aluminum have also been tested (Risha et al., 2001; Evans et al., 2004).

Emission Spectroscopy

Emission spectroscopy diagnostics enable a researcher to analyze photonic emissions by wavelength. Figure 1 shows a schematic of the inside of the Ocean Optics USB2000 Spectrometer. The spectrometer converts incoming light into voltage across a Charge Coupled Device (CCD) wherein each pixel of the CCD represents a pre-calibrated wavelength. Much like how a prism diffracts white light into the visible spectrum, a diffraction grating inside the

spectrometer expands the incoming emission, allowing each pixel of the CCD to detect a different wavelength of the incoming light. The CCD pixel produces a voltage that is proportional to the intensity of the light at that specific position, or wavelength.

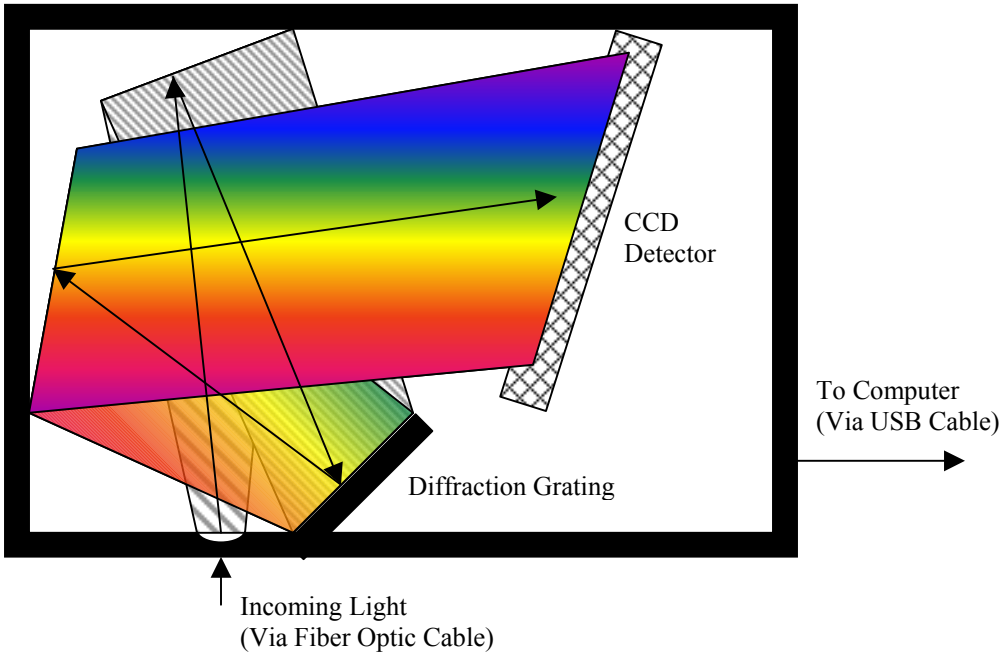

Figure 1: Spectrometer Internal Schematic

There are several features of the USB2000 spectrometer that make it advantageous to use in a strand burner environment. A key feature of the Ocean Optics product is that it is pre-calibrated and adjusted at the factory and does not need calibration (Appendix A). This reduces the amount of necessary support equipment by not needing calibration light sources and additional lab space. The Ocean Optics fiber optic cable included calibration data as well (Appendix B). Also, the USB2000 is roughly the size of a small digital camera (90mm x 65mm x 35mm) occupying very little lab space (Appendix C). The input and output signals are fiber optic and USB cables. Not relying on a complex configuration of lenses and mirrors allows the

device to be safely placed out of sight where it cannot be damaged. The simple USB interface utilizes an effective common commercial standard and does not require additional unique hardware to operate.

The compact OceanOptics USB2000 spectrometer receives its power and control signals through a USB cable attached to a PC with the SpectraSuite software installed and running. Through a graphical user interface (GUI), all spectrometer functions may be set. The data collection process is also initiated through the computer software.

Effective use of the spectrometer software allows the researcher to define the integration time for the sample. The longer the spectrometer's CCD collects photons, the higher the output voltage will be. Setting the integration time too long will cause the output of many pixels to peak at their maximum voltage output. Setting the integration time too low will result in poor Signal-to-Noise (S/N) Ratio. When all pixels are assembled graphically, the results may look similar to the curves in Figure 2. The lines both represent typical spectral data collected from two separate non-aluminized propellant samples.

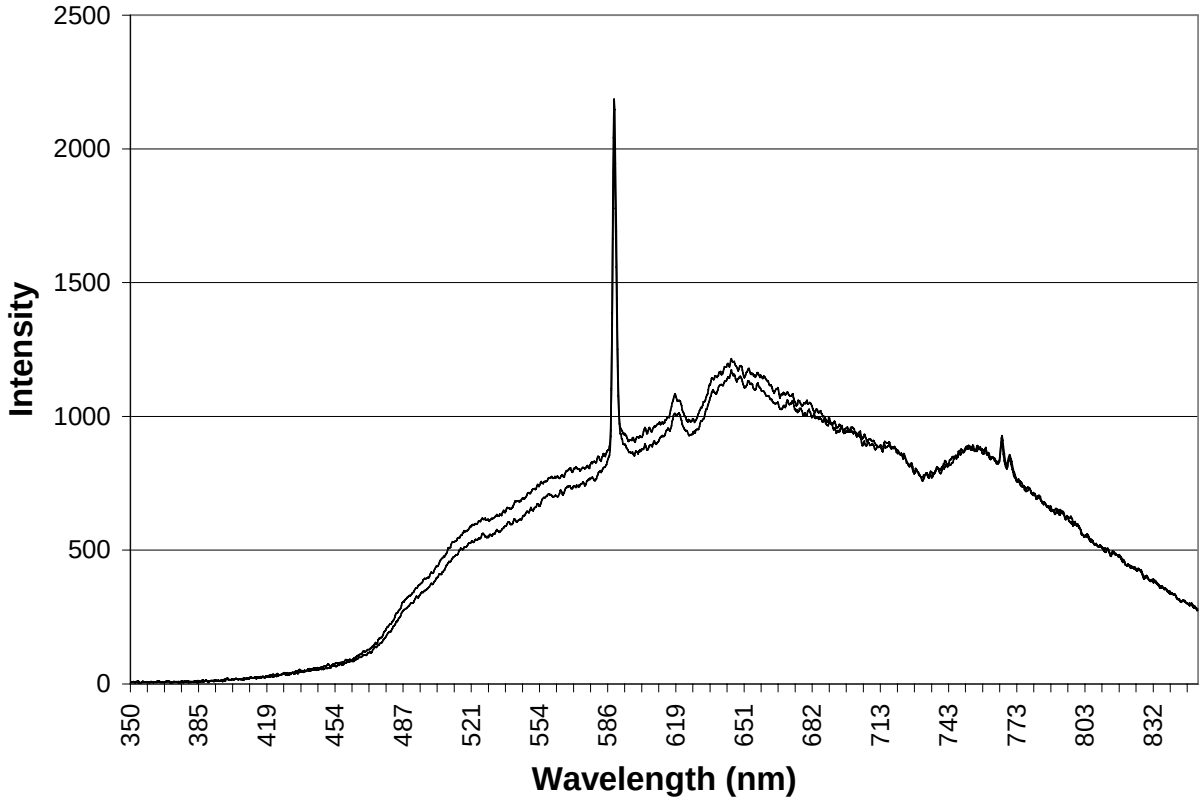

Figure 2: Typical Plot Showing Spectrometer Data: 2 Samples of Same Propellant Mixture

Through the SpectraSuite software developed by Ocean Optics, the spectrometer's manufacturer, time dependent data can also be collected. After compiling the data, changes or fluctuations within the burning region may become visible. Figure 3 shows a typical example of time-resolved emission data. The recorded intensities increase as the sample starts burning, and specific peaks become better defined. This information is discussed further in the results section.

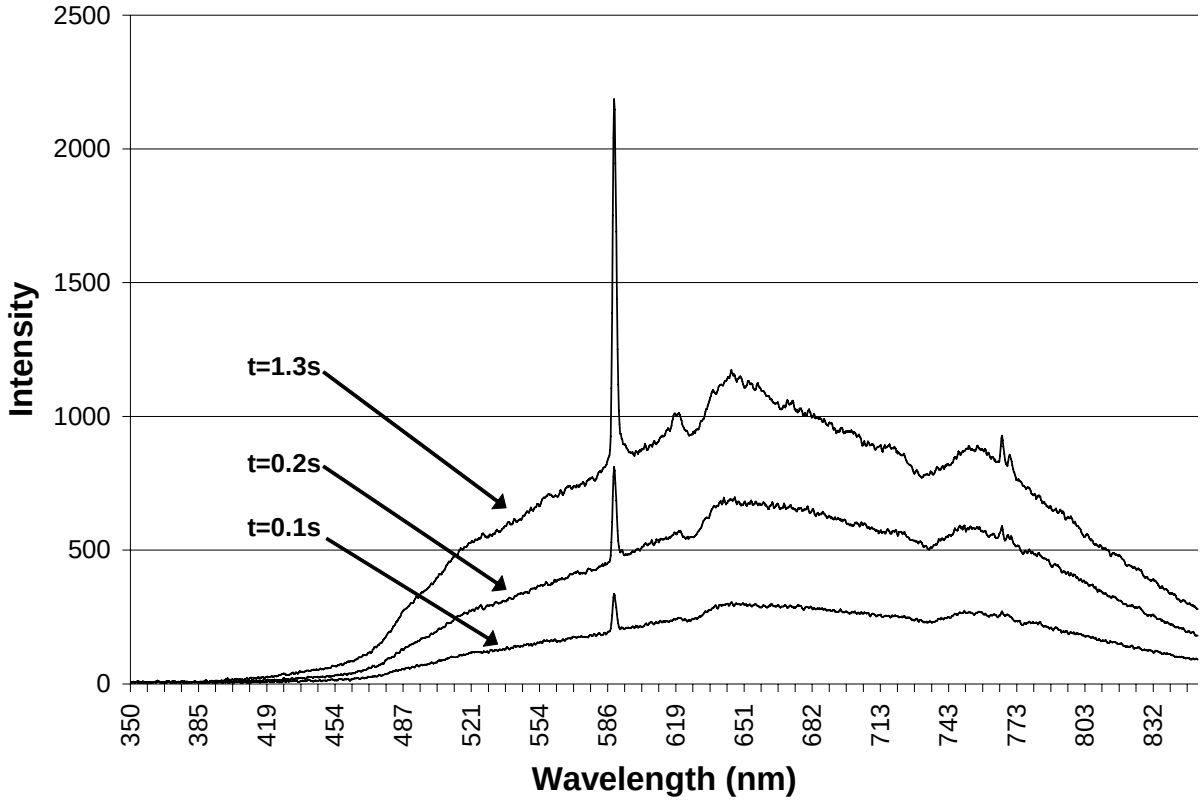

Figure 3: Time-Resolved Spectrometer Plot

Emission spectroscopy is useful to solid propellant research in that the diagnostic can assist in the identification of combusting species. Elements or compounds within the propellant, when excited, heated or decomposed give off unique spectra (Arvanetes and Petersen, 2006). Looking at Figures 2 and 3, there are several specific peaks that occur across the spectrometer's wavelength range. References such as Schick's *Thermodynamics of Certain Refractory Compounds Volumes 1 and 2* (1966), *The Handbook of Chemistry and Physics*, and Herzberg's *Molecular Spectra and Molecular Structure* can be utilized to identify the materials present. When modifying the propellant or adding new components, emission spectroscopy can be

employed to validate whether the additional chemical species is reacting within the combusting products.

The emission spectroscopy diagnostic can be incorporated into a combustion experiment several ways. One method is reacting solid propellant components in a Bunsen-type flame (Mamen et al., 2005). Other researchers have utilized a pressure vessel with a window allowing a profile view of the burning sample (Weiser and Eisenreich, 2005; Yang et al., 2005). This configuration is most similar to the current experiment configuration at UCF.

Emission spectroscopy is also applicable to hybrid rockets. The spectrometer apparatus can be applied in a manner to allow internal combustion monitoring (Wright et al., 2005) or to study the exhaust plumes (Maxwell and Hudson, 2005; Hudson et al., 1998). In another experiment, researchers intended to target carbon dioxide, water, and hydroxyl (OH) radicals in the exhaust of a hybrid rocket. The experimental setup incorporated two spectrometers detecting different spectral ranges (Wilson et al., 2005).

Optical diagnostics other than emission spectroscopy have also been employed, enabling researchers to study combustion features such as how far above the surface of a burning propellant sample different species react (Parr and Hanson-Parr, 2000). Lasers and advanced absorption techniques were employed to identify where and how various components react with each other.

CHAPTER THREE: EXPERIMENT

Prior to burning a sample, the propellant must first be prepared. The required quantities of ingredients are carefully combined utilizing a vacuum pump to ensure all air bubbles are removed from the propellant. A small amount of curative is added near the end of the mixing process to cause the binder to solidify. The final mixture is extruded into narrow tubing, allowing the propellant to cure. The tubing containing the propellant is cut into shorter lengths, roughly 30cm long and placed into a constant temperature oven to cure at the specified conditions. Once cured, the propellant is removed from the tubing. These propellant strands are stored until needed.

All ingredients for the mixtures are obtained from commercial suppliers. Table 1 provides a list of the primary chemicals. Note that only monomodal ammonium perchlorate (AP) was purchased, with an average size of 200μm. For bimodal AP, the coarse powder is ground in a ball mill and sifted through a sequence of mesh screens. The fine AP used in the experiments has a mean diameter of 82.5μm ±7.5μm (Stephens et al., 2005b). The aluminum has an average size of 3 μm. Note also that the PAPI 94 curative, an MDI, is a room-temperature curing agent. The IPDI curative requires a slightly increased temperature for curing.

Table 1: Propellant Ingredients, Details, and Suppliers.

Type	Name	Supplier	Notes:
Aluminum Powder	German Black	FireFox Enterprises	3 micron
Ammonium Perchlorate	-	SkyLighter	200 micron
Fe_2O_3	microfine	FireFox Enterprises	325 mesh
HTPB	R-45M	Aerocon Systems	-
Diphenyl Methane Diisocyanate (MDI)	PAPI 94 (DOW)	Aerocon Systems	-
Isophorone Diisocyanate (IPDI)	-	SkyLighter	-

At the center of the experiment is the strand burner. This pressure vessel allows propellant samples to be safely tested in a controlled environment.

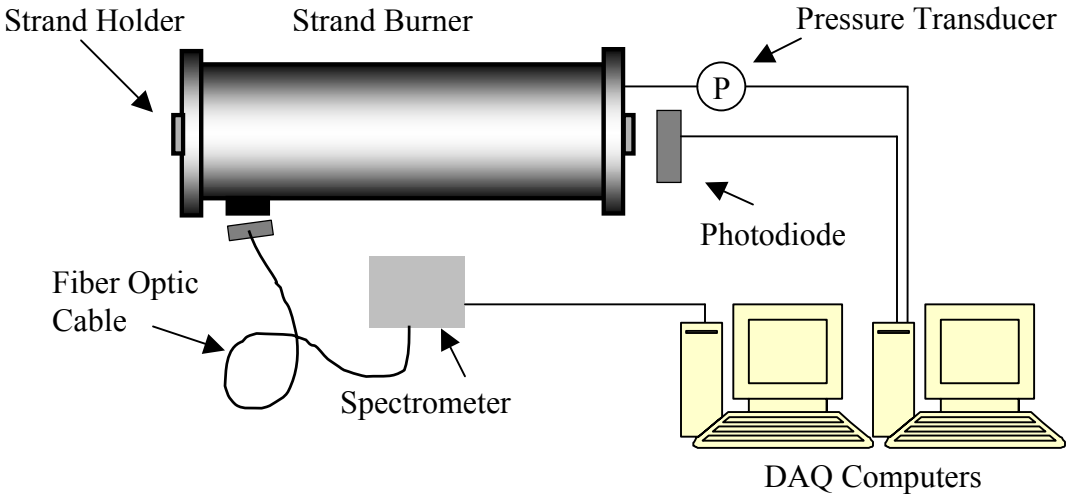

Figure 4: Schematic of Strand Burner Experiment

Figure 4 shows a schematic of the strand burner facility and related diagnostics, discussed in more detail by Carro et al. (Carro et al., 2005) and Stephens et al. (Stephens et al., 2005a). The burner is made of a cadmium-plated, low-carbon steel alloy and is capable of test pressures up to 5300 psi; it has an inner diameter 7.94 cm and is 30.48 cm long. Each propellant sample is 6.4 mm in diameter and approximately 25.4 mm in length. Burn rate is measured in each experiment from the rise in chamber pressure as recorded by the pressure transducer and verified by the visible light emission monitored by the photodiode mounted near the endwall opposite the burning sample (Fig. 4).

The strand requires minimal preparation for burning. The strand is placed into the strand holder, as shown in Figure 5. The sidewalls of the propellant are coated with HTPB to inhibit combustion on the sides, forcing the strand to burn from along its axis. A 30-gauge Nichrome wire is placed across the leading edge of the propellant sample and secured to the eyelets on either side of the sample. The Nichrome wire is the propellant ignition source.

Figure 5: Propellant Strand Prepared in Strand Holder

Solenoid-operated pneumatic valves control the filling and venting of the gases to and from the bomb, ensuring remote operation. Manual valves and metering valves provide redundancy and preset flow control. A removable plug manufactured from a 25.4-mm (1-in) diameter bolt serves as the propellant sample holder, which contains a Conax feed-through fitting for passage of the main ignition wire. Ignition of a strand is done by passing a current through a nichrome wire strung across the main ignition lead, touching the propellant, and connected to the grounding eyelet, as shown in Figure 5. An off-the-shelf motorcycle battery provides the current. A relay in between the battery and the propellant sample is connected to an ignition switch for remote firing.

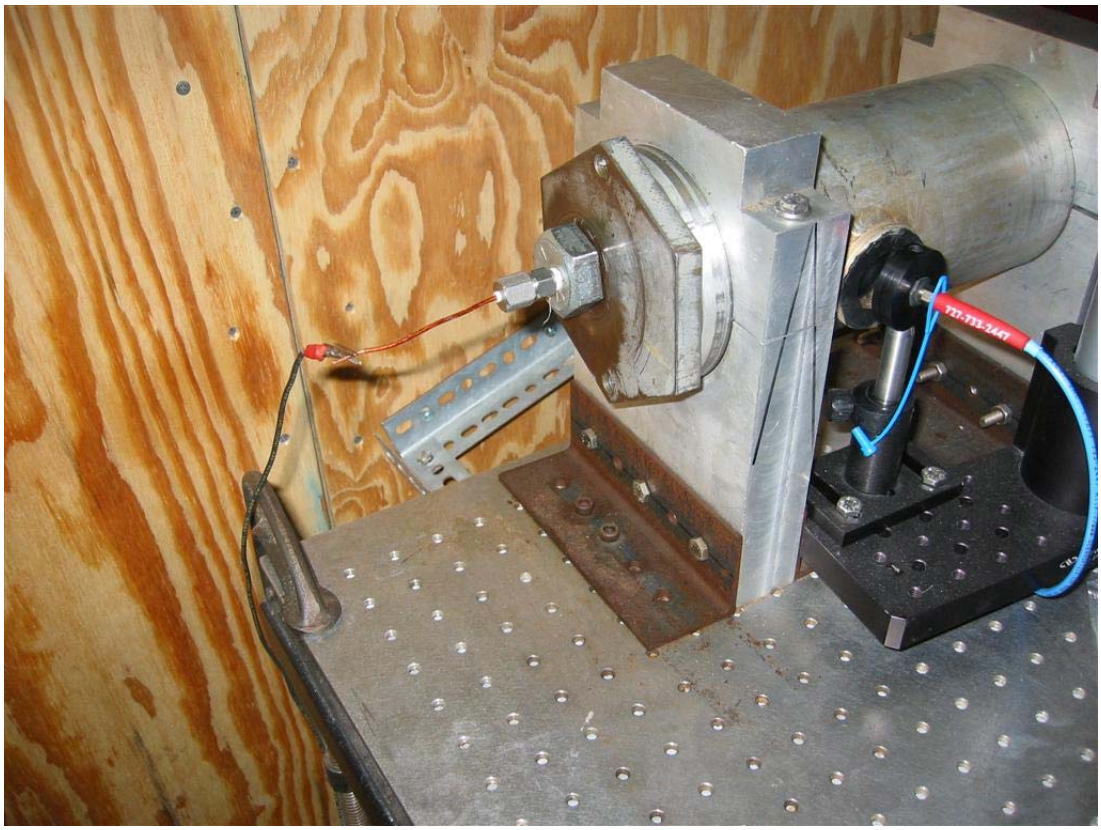

Figure 6: Fully Prepared Strand Burner

The assembled strand holder is placed into the strand burner and secured. The ignition source is connected and the room is vacated. Figure 6 shows the strand burner with the strand holder installed and the ignition source connected. From a remote location, the strand burner is pressurized to the required level with Argon gas. The data acquisition systems are activated, and the ignition signal is sent. From the remote location, ignition is verified through a real-time data display of the chamber's pressure. Upon completion of data acquisition, the chamber is depressurized and the next sample is prepared.

Three primary diagnostic techniques are available for monitoring the burning of a sample: pressure, light emission, and spectroscopy. A schematic of the diagnostics relative to the bomb is provided in Figure 4. The pressure transducer (Omega model PX02C1-7.5KG5T) is mounted in the endwall opposite the sample and serves as the primary means for obtaining the burn rate; the range of the transducer is 1-510 atm (0-7500 psig). A secondary technique for quantitative assessment of the burn rate is based on the detection of the visible light emitted from the burning sample. The high-speed Silicon-photodiode detector (New Focus 2031) is positioned near the window plug on the far-side endcap (Fig. 4). For the experiments herein, the light emitted from the burner was not spectrally filtered so that the Silicon detector observed broadband emission over its entire spectral range, which is approximately 350-650 nm. Such broadband emission provides a clear beginning and end of the propellant burn. The third diagnostic, the spectrometer, utilized in the current setup is positioned at the sidewall, in-line with the sample. The compact spectrometer is an Ocean Optics USB2000 device (Fig. 7) that plugs directly into the computer via a USB port, as mentioned in Chapter 2. The emitted light from the burning sample is passed to the spectrometer via a fiber optic cable (Fig. 6). The spectrometer is controlled and powered through the computer's USB port. The spectrometer and

related software allow for efficient and accurate data collection at 100-millisecond intervals (Arvanetes et al., 2006).

Figure 7: An Ocean Optics USB2000 Spectrometer

During the course of an experiment, in addition to the pressure transducer and broadband intensity data, the time-dependent spectra are obtained and subsequently analyzed and compared to the growing database of spectra for the propellant combinations previously studied in the laboratory. The spectrometer is blazed for a wavelength range from 200 – 800 nm. This spectral range allows access to many intermediate and stable species within the flame zone, with emphasis on those formed from their solid-particle precursors. For example, a typical wavelength range and species within the visible operating range of the spectrometers when aluminum particles are present would be the A→X emission of AlO near 480 nm (Sultzmann,

1975; Linton and Nicholls, 1969; Ye et al., 1988). When additives are present, similar intermediate oxides are monitored, depending on the additive of interest.

When the propellant sample burns within the pressurized strand burner, the hot, gaseous combustion products create an increase in pressure during the course of the burn due to the gaseous products and the higher temperatures. This pressure increase was typically about 10-20% of the initial pressure. Although ideally the samples should be burned in a constant-pressure environment, this slight increase in pressure created a means with which to quite accurately determine the burn rate of a given strand. Figure 8 presents a typical pressure signal showing the condition before, during, and immediately after a test. The start of the pressure rise clearly delineates the onset of burning; upon completion of the burning, there is a distinct inflection point in the pressure and then a slower decrease in pressure until an equilibrium pressure level is attained. The equilibrium pressure level corresponds to the pressure due to the initial argon diluent plus the additional gases from the combustion products. The decrease in pressure immediately upon completion of the burn is reasoned to be from heat transfer, as the gases will begin to cool once the burning has stopped. It could also be due to condensation of the particulate matter upon cooling.

A computer model was created using MathCAD to confirm the trends observed in the pressure traces (Appendix D). Using conservation of energy and conservation of mass in an unsteady control volume approach, the model supports the burn data. The model accurately predicts the pressure rise recorded in actual experiments. Future experiments can benefit from the model through accurately projecting how a newly developed fuel will react and the pressure rise to be expected from a given sample size.

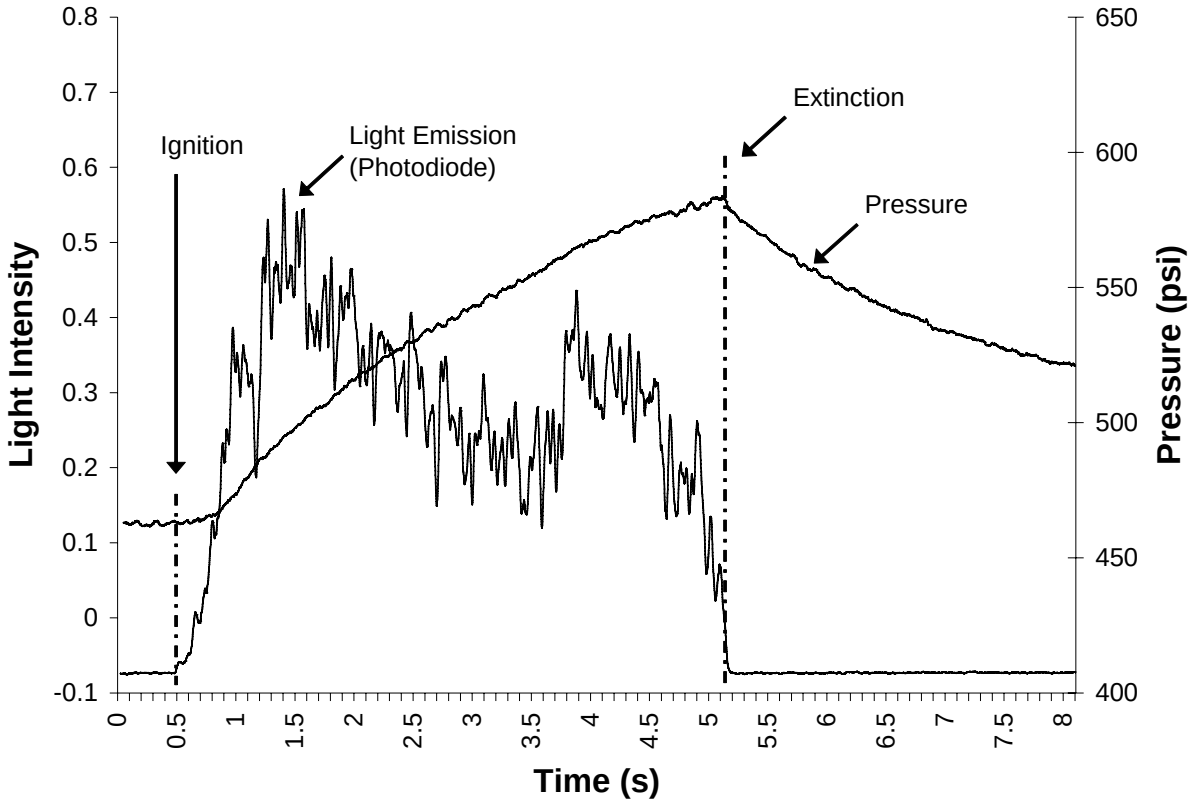

Figure 8: Typical Pressure and Photodiode Emission Signals

The photodiode signal corroborates the onset and completion of the burning as inferred from the pressure trace. Figure 8 shows that the light increases immediately upon initiation of the burn and ends when the burning has finished. In many cases, the light intensity decreased with time and is most likely due to solid particulates obscuring the visible emission from the gaseous products. The burn rate inferred from the emission signal in most cases was within a percent or two of the rate inferred from the pressure signal. In certain cases where there is a problem with the pressure signal transmission, the burn rate can be taken from the light signal with confidence. A closer look at the light and pressure signals during the actual burn is shown in

Figure 9. The burn time is indicated, and the quality of the data seen in Figure 9 is representative of most burns.

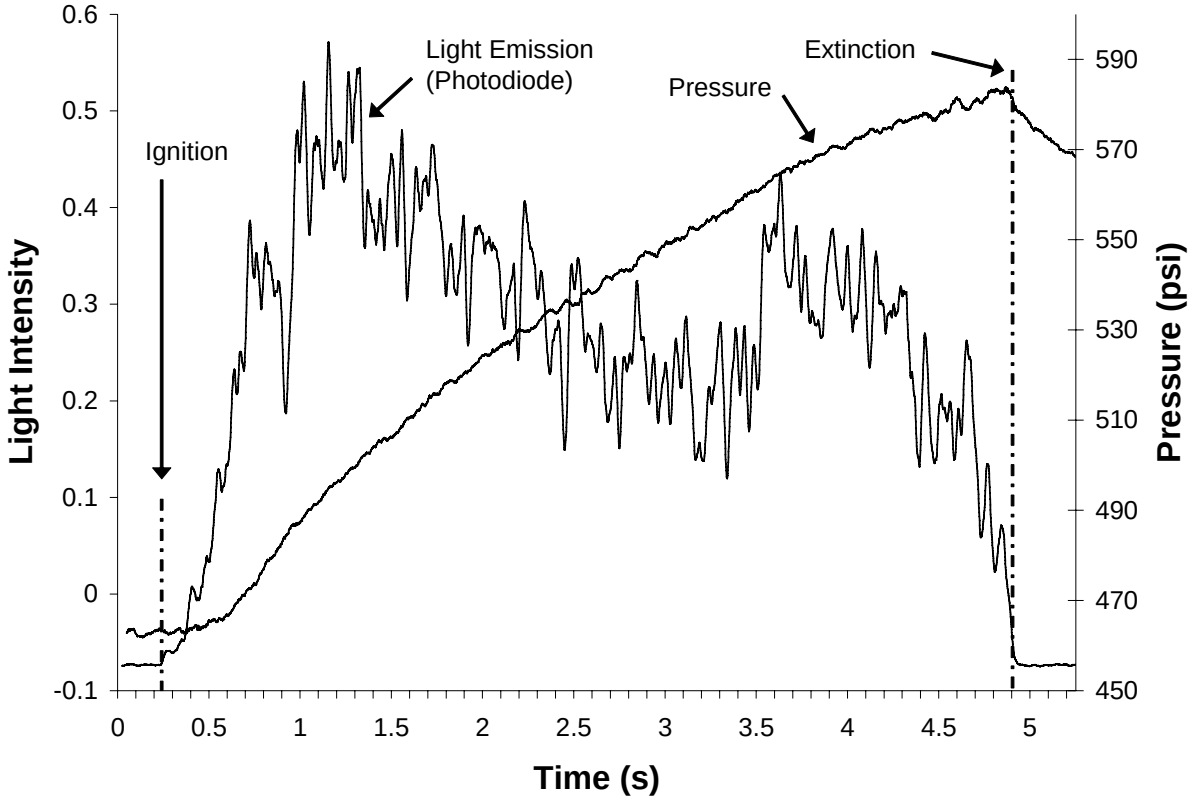

Figure 9: A Detailed Look at Pressure and Emission During a Burn

Ignition occurs at the point when the chamber pressure begins to increase. At the onset of ignition, the propellant begins to emit light which is measured through the photodiode. Burn rate calculations for the samples above (Figs. 8 and 9) are conducted as follows:

$$t_{ignition} = 0.2300s$$
$$t_{extinction} = 4.9100s$$
$$length = 1.1110in$$
$$r = \frac{length}{t_{extinction} - t_{ignition}} = 0.2374\frac{in}{s}$$

CHAPTER FOUR: RESULTS

The experiment consists of several complementing investigations. Prior to the current effort, many of the propellants developed contained aluminum. Since, as previously discussed, aluminum is the preferred metallic fuel; a spectral study of a baseline aluminum fuel was desired. The most recent efforts in the lab have focused on non-aluminum based propellants. The significant differences between these two propellants lends itself to a potentially interesting comparison – what effect does the aluminum have on the emission spectra of a composite rocket propellant? A bimodal variant of the AP/HTPB fuel was also developed.

The addition of an emission spectroscopy diagnostic with the ability to collect time-resolved data during the course of a burn can present a better understanding of how a reaction develops inside the strand burner. The broadband emission data collected at the far side end cap has traditionally been compared with the pressure data to corroborate ignition and extinction times. A typical experimental problem occurring with some propellants is premature explosion. Explosions are fairly easy to identify on the pressure transducer's output, but what is actually happening is not very clear. With the addition of an emission spectroscopy diagnostic, a better insight to the phenomenon is possible.

The diagnostics, when combined, provide a detailed account of the bulk chemical reactions within the strand burner. The results section is broken into seven separate investigations.

Al/AP/HTPB Baseline Propellant Study

Table 2 identifies the composition of a typical baseline, aluminized propellant.

Table 2: Al/AP/HTPB Baseline Propellant Formula

	HTPB	Tepanol	Al (3μm)	Fe2O3	AP (200μm)	Curative
Mix 044	10.55%	0.20%	19.98%	0.50%	67.32%	1.45%

The propellant strands were tested at eight pressure intervals ranging from 250psi to 2000psi. The pressure data are utilized to calculate burn rate. The light emission data assists with validating ignition and extinction.

Burn rate calculations are made for each sample throughout the target pressure range and plotted on a log-log plot. An exponential curve is fit to the data, and the coefficient (A) and the pressure exponent (n) can be calculated. In Figure 10, a pressure exponent of 0.60 is calculated with an R^2 value of 0.9512. The three outliers were from samples that unexpectedly exploded during the burn. In a later section, identification of exploding propellant samples is discussed.

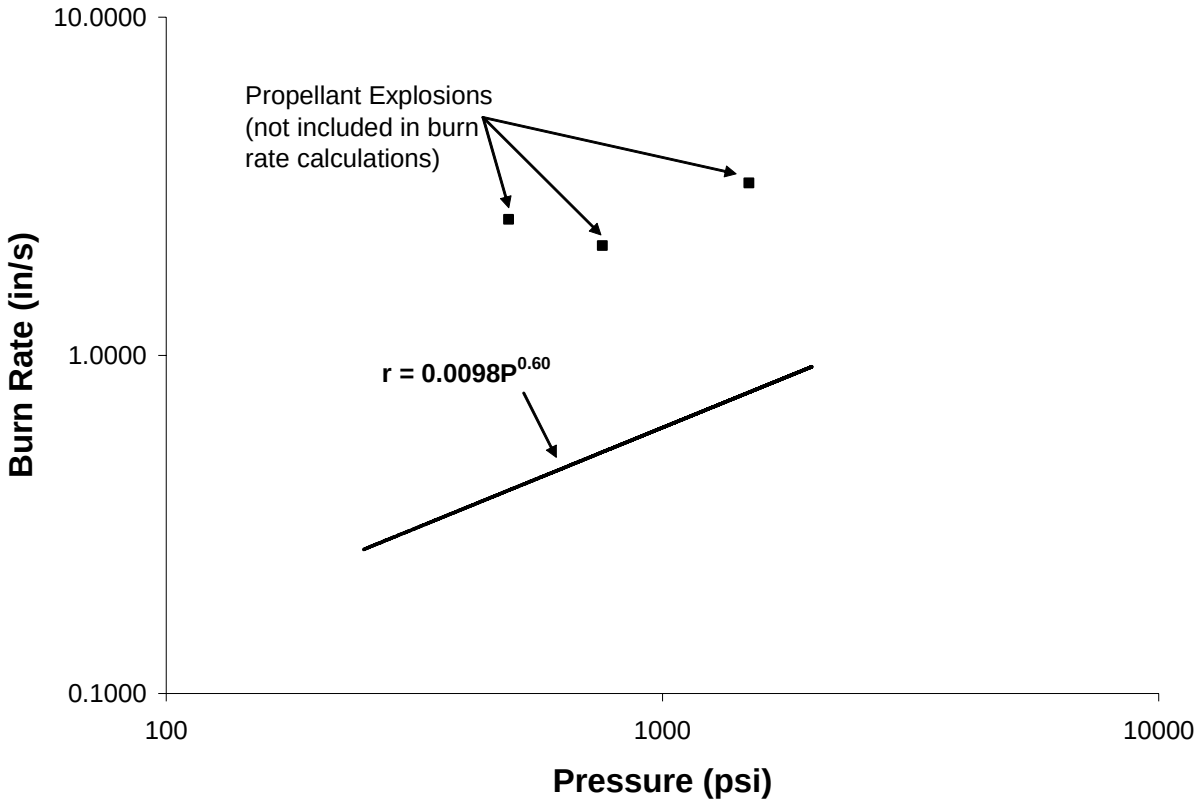

Figure 10: Burn Rate Data for a Baseline Al/AP/HTPB Propellant

The spectrometer data collected from several Mix 044 burns show several distinct peaks. (Fig. 11). Each of the four curves in the Figure represents the peak emission spectra from one of four separate burns within the same batch of propellant.

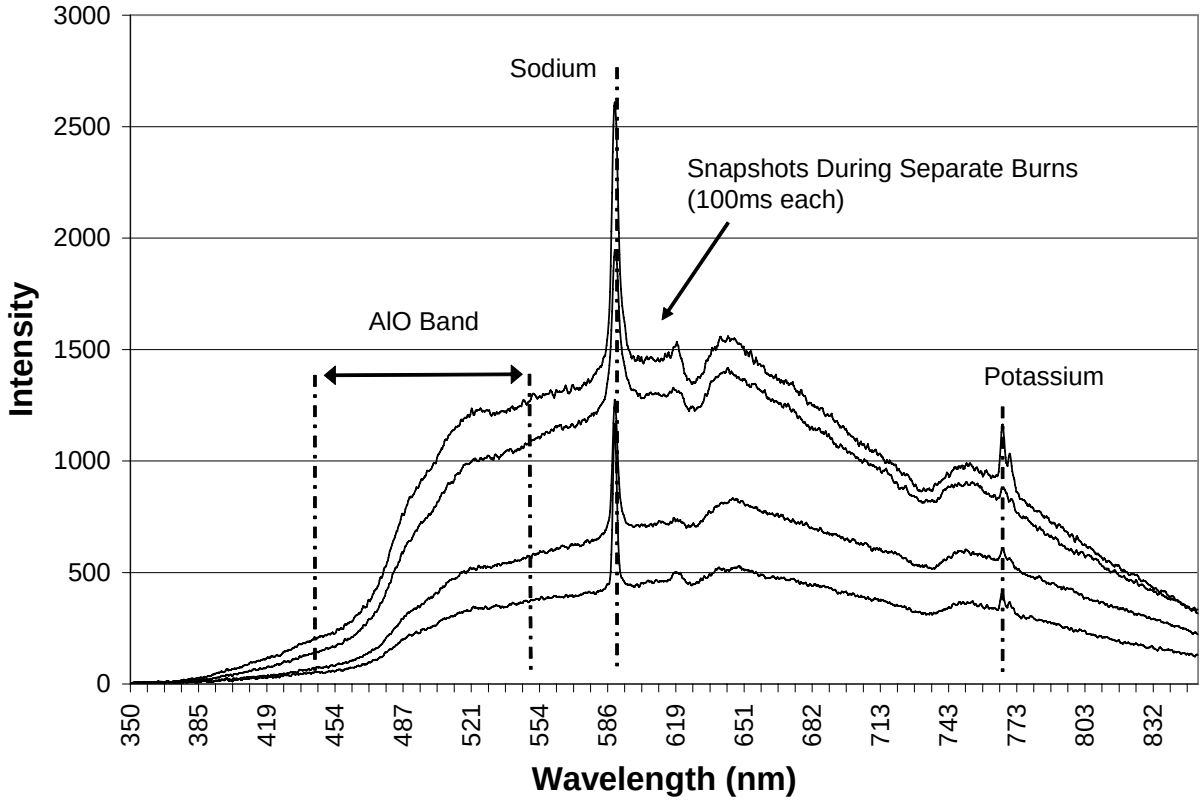

Figure 11: Emission Spectra for Aluminized Baseline Propellant

The most visible peak is centered at 589nm. Recent research has attributed this feature to sodium pollution (Maxwell and Hudson, 2005). Similarly, research shows the emission at 767nm is due to potassium. These pollutants are routinely found in current research, and their intensity relative to the other emissions is comparable. This is not an unexpected result. The pollutants are most likely contained within the AP and/or HTPB. The aluminum does not contain the sodium or potassium pollution due to the existence of the same emission features in both aluminized and non-aluminized propellant samples. Through further testing, the responsible ingredient, AP or HTPB, for the recorded pollution can be identified, although it is

likely to be the HTPB as Maxwell and Hudson (2005) see it in their HTPB-only hybrid rocket burns.

AP/HTPB Baseline Propellant Study

Table 3 identifies the composition of a typical baseline aluminized propellant.

Table 3: AP/HTPB Baseline Propellant Formula

	HTPB	Tepanol	Al (3μm)	Fe2O3	AP (200μm)	Curative
MDA02	18.07%	0.20%	0.00%	0.00%	80.00%	1.73%

Non-aluminized propellants are not expected to have comparable combustion characteristics. The explosive nature of aluminum powder promotes a faster burn rate but introduces increased sensitivity to smaller pressure changes. Figure 12 is the non-aluminized pressure and photodiode data.

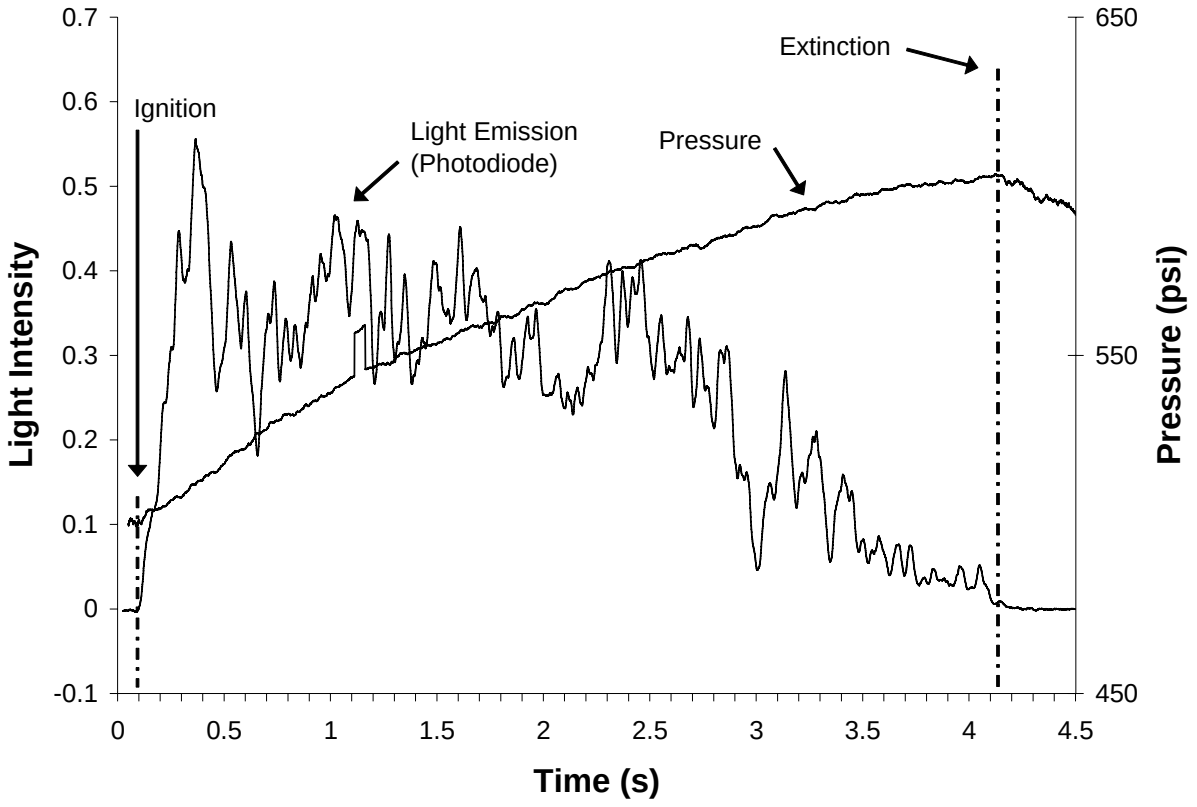

Figure 12: Pressure and Light Emission - AP/HTPB Baseline

The pressure spike around the 1.25 second mark is from the electromagnetic interference induced by the ignition source relay. Many plots show this feature and the event is ignored. Non-aluminized propellants appear to be more stable than an aluminized counterpart. The pressure exponent derived from the burn rate plots qualifies the stability of a propellant. When testing an AP/HTPB baseline propellant, the pressure exponent is approximately half (0.29 vs. 0.60) that of an Al/AP/HTPB baseline propellant with monomodal AP and 3-μm Al. (Fig. 13)

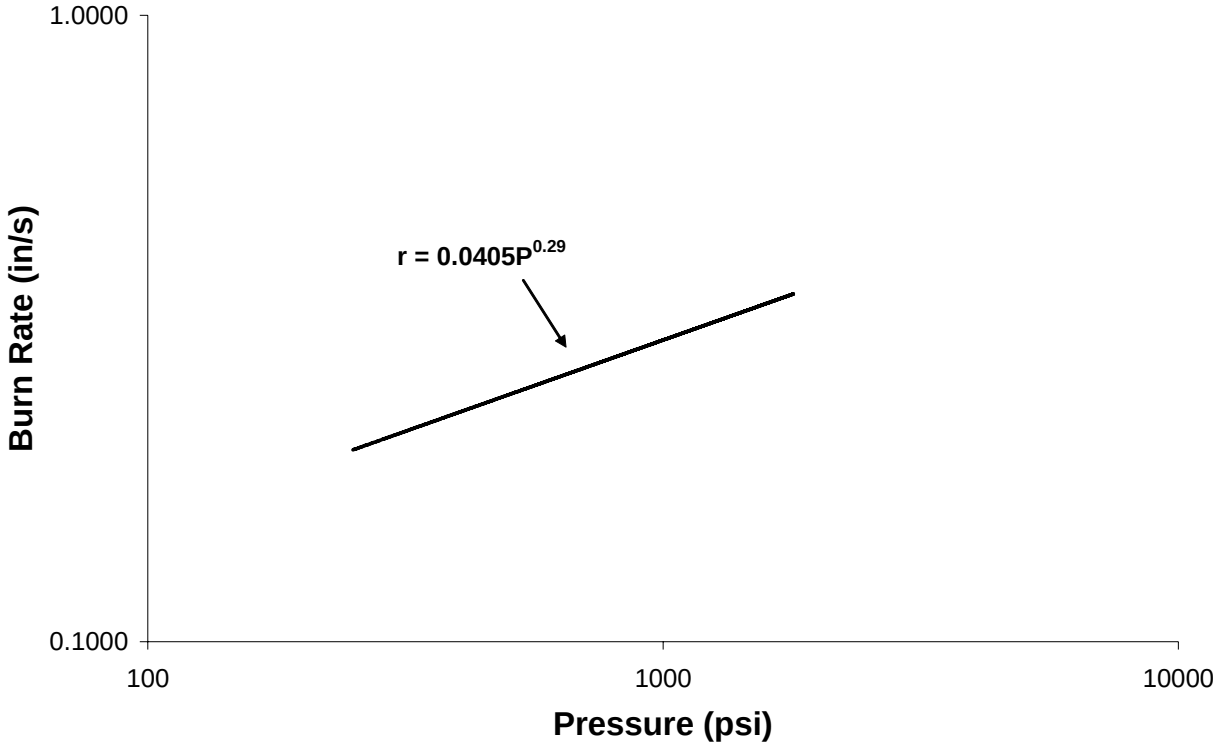

Figure 13: Burn Rate Data for Baseline AP/HTPB Propellants

In regards to emission spectroscopy, the absence of aluminum combustion was expected. The data collected continued to show the same sodium and potassium emission features. (Fig. 14) The two curves in Figure 14 depict separate burn samples from the same batch of non-aluminized baseline propellant.

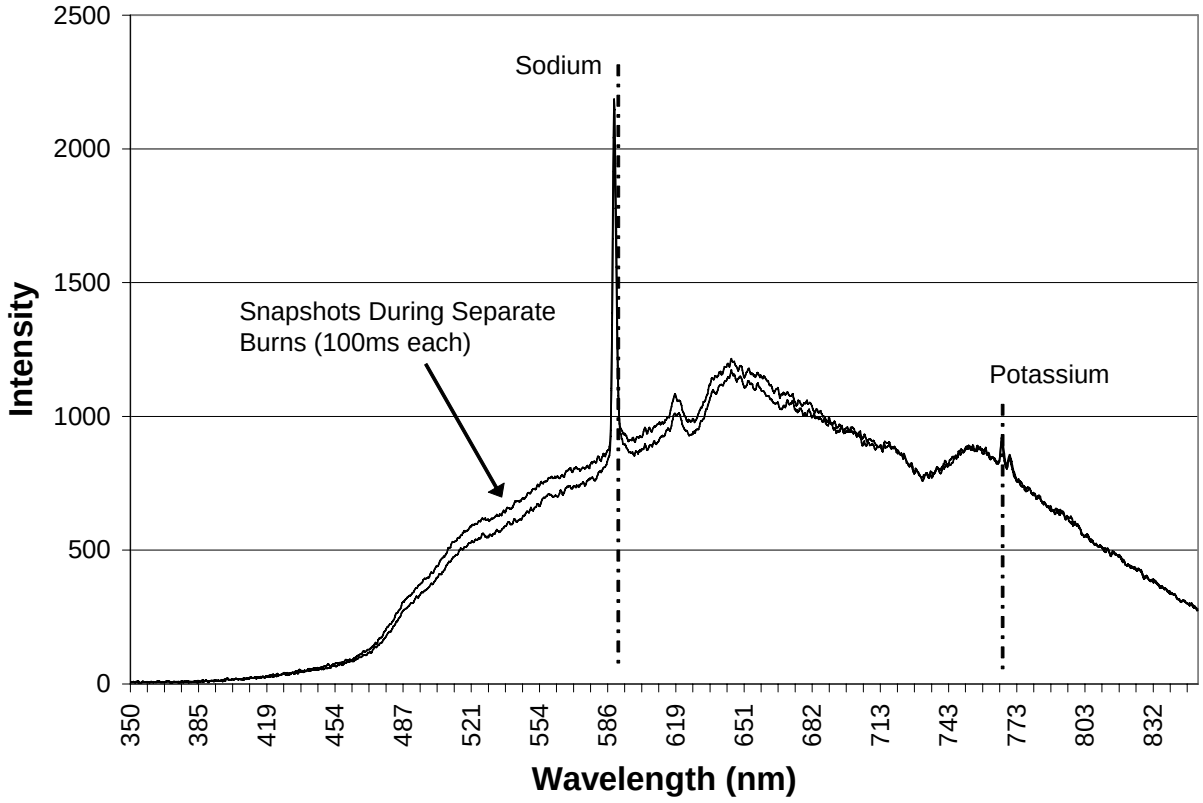

Figure 14: Emission Spectra for AP/HTPB Baseline Propellants

Bimodal AP/HTPB Propellant Study

Table 4 identifies the composition of a typical baseline aluminized propellant.

Table 4: Bimodal AP/HTPB Propellant Formula

	HTPB	Tepanol	Al (3μm)	Fe2O3	AP (200μm)	AP (82.5μm)	Curative
MDA04	18.07%	0.20%	0.00%	0.00%	56.00%	24.00%	1.73%

The addition of bimodal ammonium perchlorate (AP) to an Al/AP/HTPB propellant has previously been attempted with promising results (Stephens, 2005b). The pressure and light traces, Figures 15 and 16, depict a smooth and consistent burn.

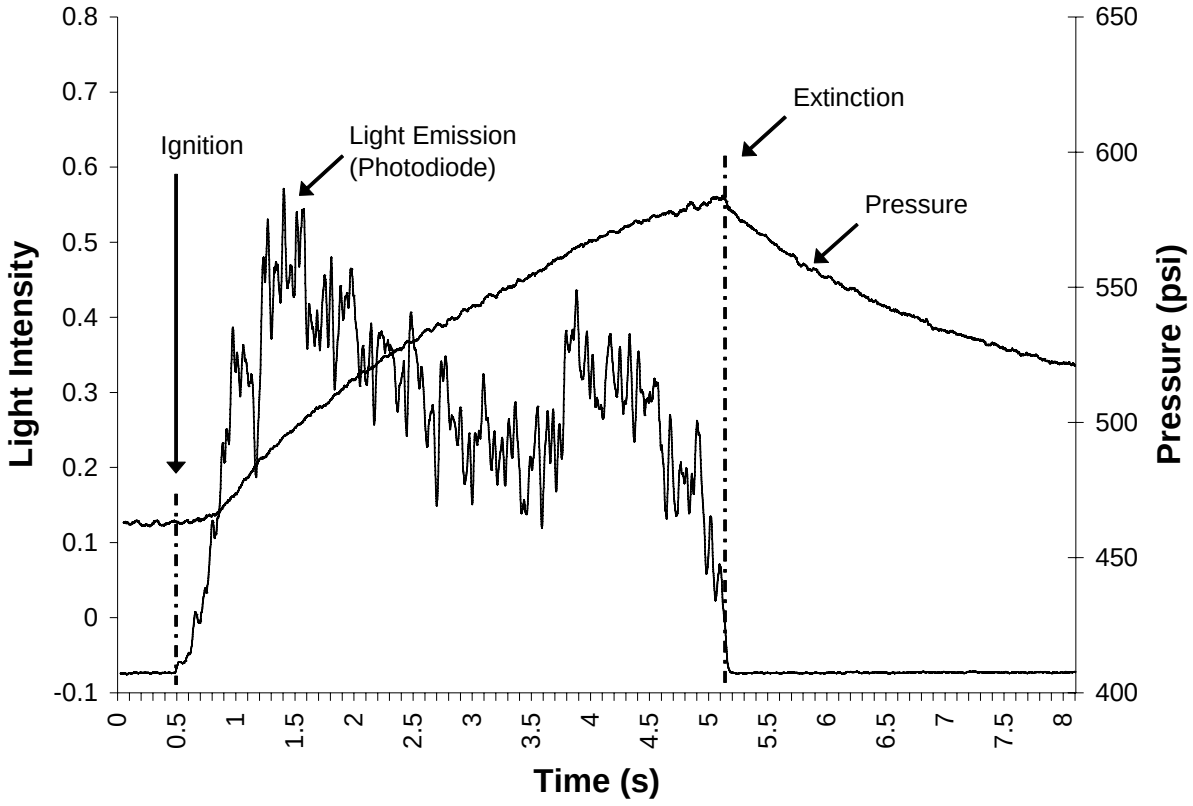

Figure 15: Pressure and Light Emission - Bimodal AP/HTPB

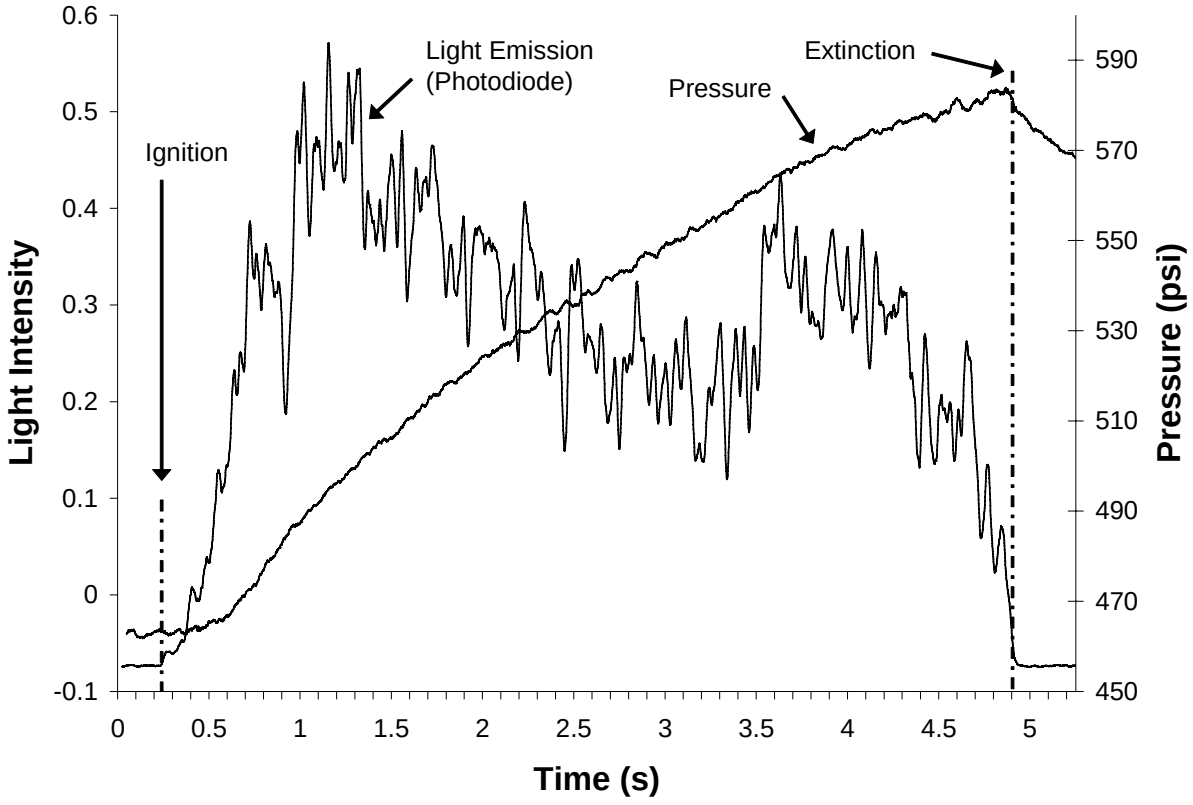

Figure 16: Pressure and Light Emission - Bimodal AP/HTPB - Detailed View

Over a pressure range of 250 to 1500 psi, the individual burn rates were calculated and plotted on a log-log graph as shown in Figure 17.

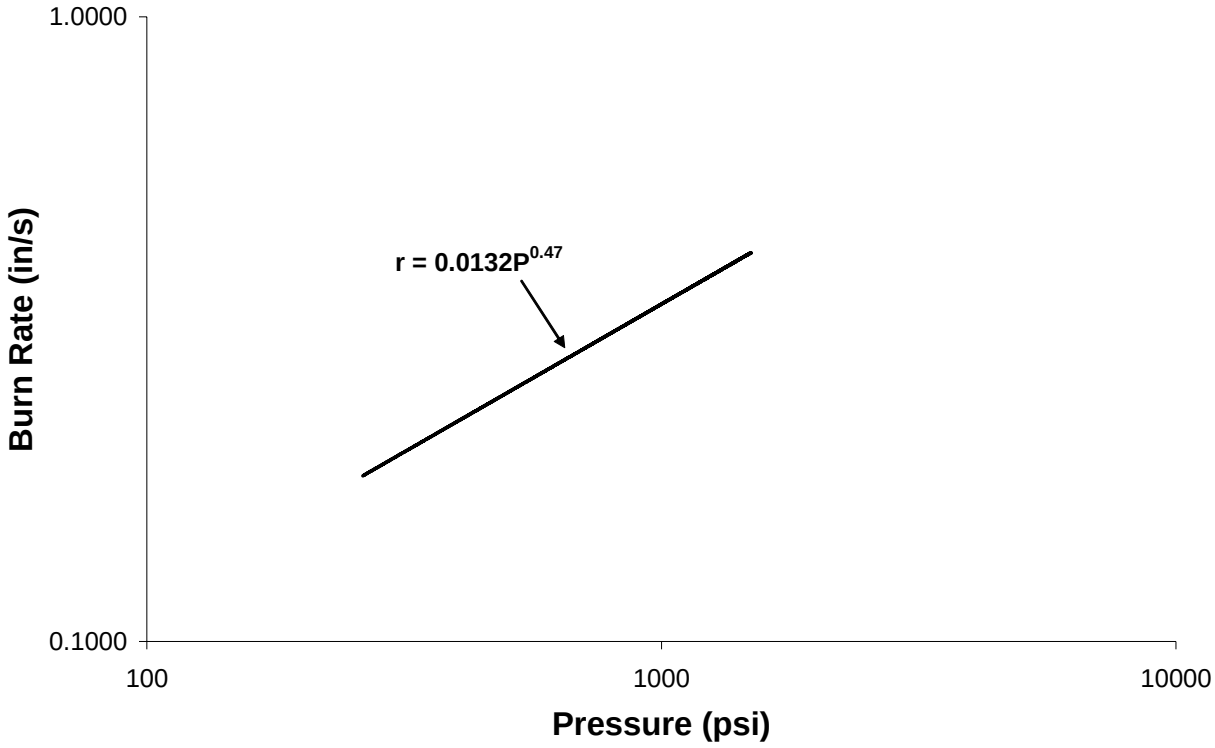

Figure 17: Burn Rate Data for Bimodal AP/HTPB Propellant

By comparison, the pressure exponent is higher than that of the baseline propellant but lower than the aluminum-based fuel. In the bimodal fuel, 30% of the AP consisted of particles with a mean diameter of 82.5μm ±7.5μm. The remaining 70% of the oxidizer was identical in size to the baseline propellant (200μm). Smaller particles create larger exposed surface areas, increasing the propellant's ability to burn more quickly. The addition of nanometer particles of aluminum to rocket fuel as in previous research has attempted to accomplish the goal of increasing the burn rate of a propellant formula (Stephens, 2005a). As evidenced by an increased pressure exponent, the smaller particles create a propellant that is more sensitive to pressure fluctuations.

In regards to the spectrometer diagnostic, the resultant output was expected to be similar to the baseline samples. There was no change in chemistry other than a portion of the oxidizer having a smaller particle size. The two traces in Figure 18 show data collected from the spectrometer during two sample burns of the bimodal AP/HTPB propellant. Many of the same trends and peaks are evident.

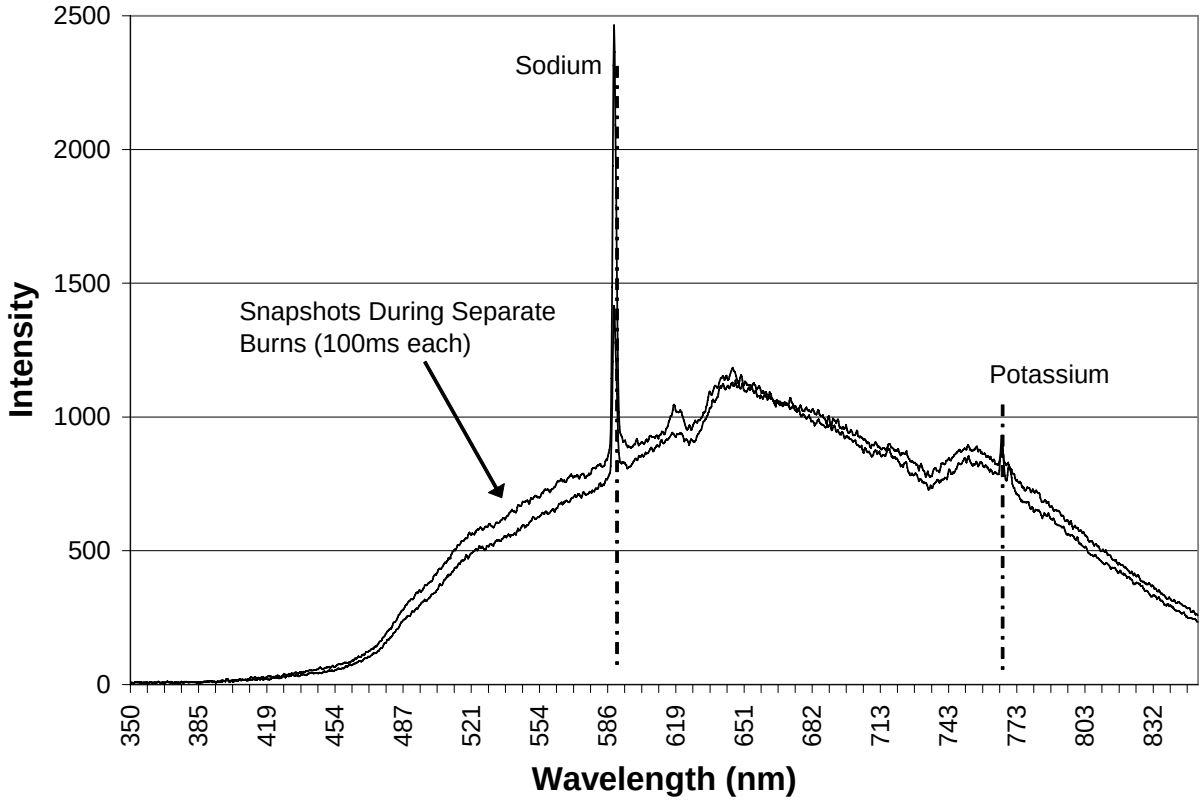

Figure 18: Emission Spectra for Bimodal AP/HTPB Propellant

AP/HTPB Propellant Comparison: Baseline vs Bimodal

After collecting data from three primary propellant compositions, a cross comparison analysis was necessary. The first comparison is between the non-aluminized propellants and the effect of the bimodal AP substitution.

As shown in Figure 19, the bimodal propellant's burn rate is higher than that of the baseline propellant at pressures above 500psi.

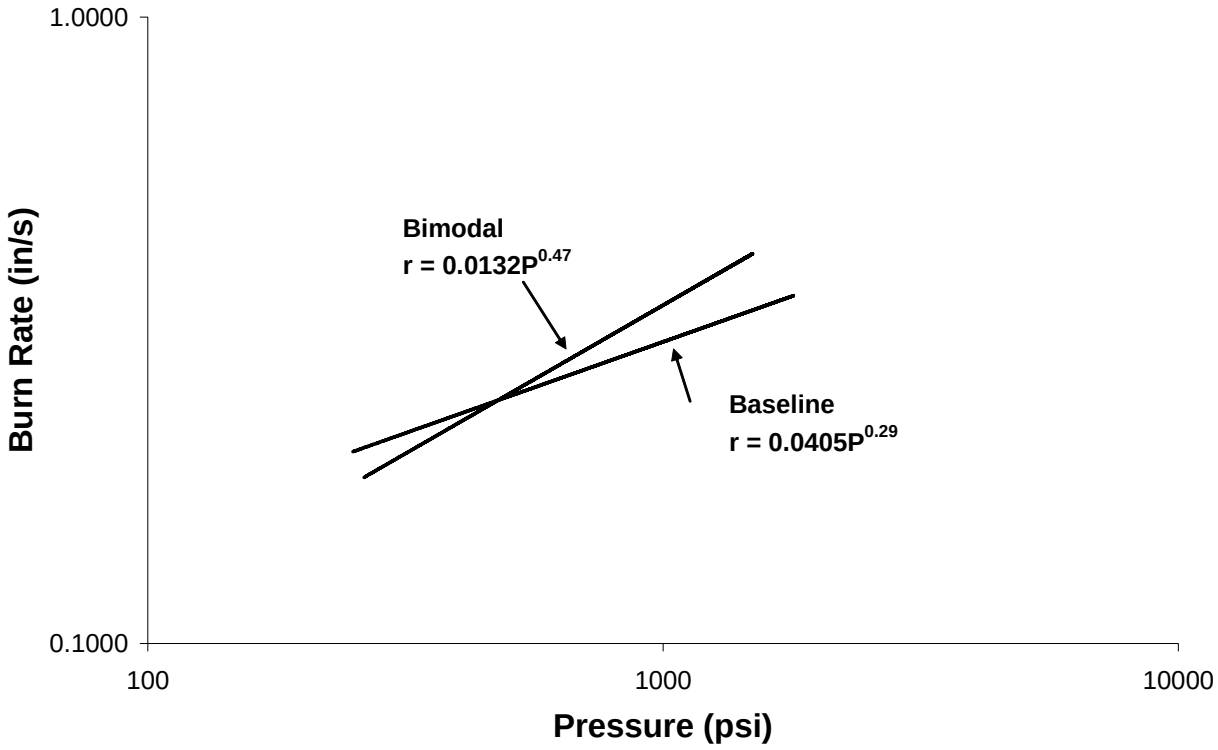

Figure 19: Burn Rate Comparison of AP/HTPB Propellants - Baseline vs. Bimodal

By inspecting the emission data collected by the spectrometer (Fig. 20), the spectra is practically identical, which agrees with the anticipated results, since there were no chemical

changes to the propellant that would induce the spectra to vary. The black traces represent the baseline composition. The gray traces represent the bimodal variation of the baseline.

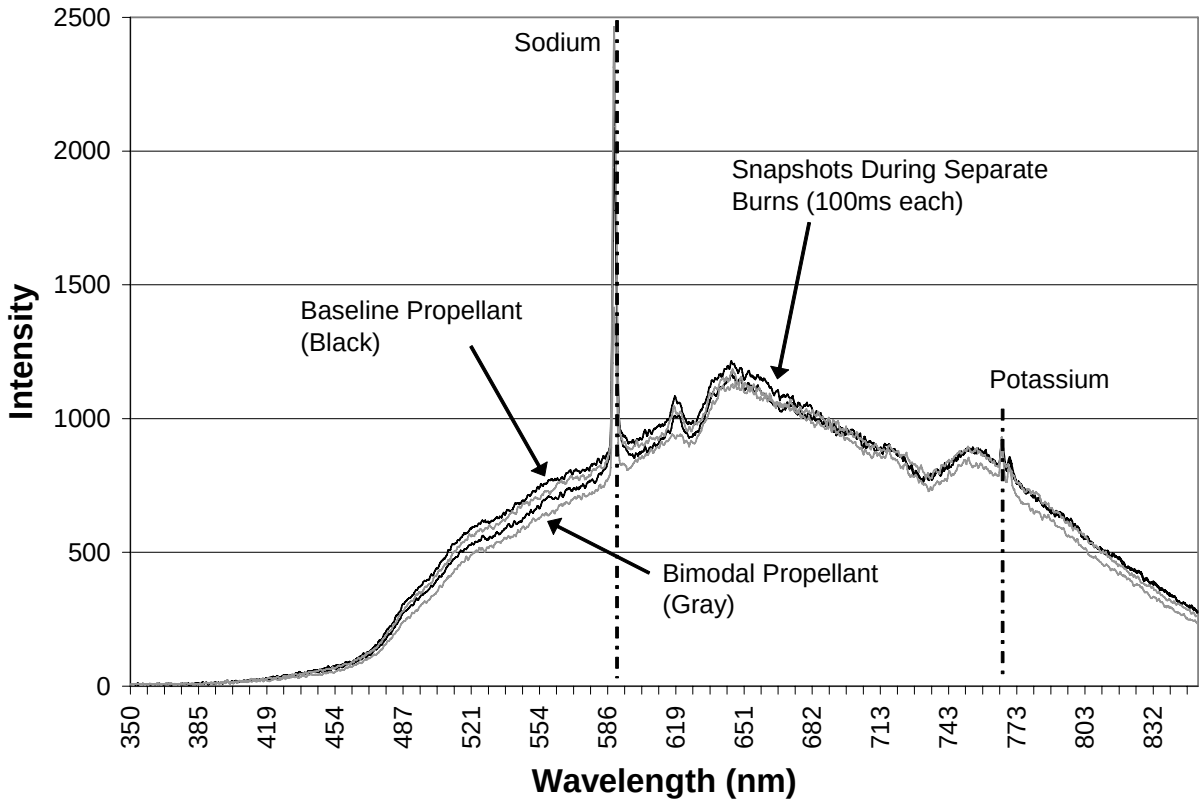

Figure 20: Comparison of Baseline Monomodal AP Propellant with Bimodal AP

The Effect of Aluminum on Baseline Propellants

The next comparison investigates how adding a fine aluminum powder to the AP/HTPB propellant changes the burn rate and emission spectra.

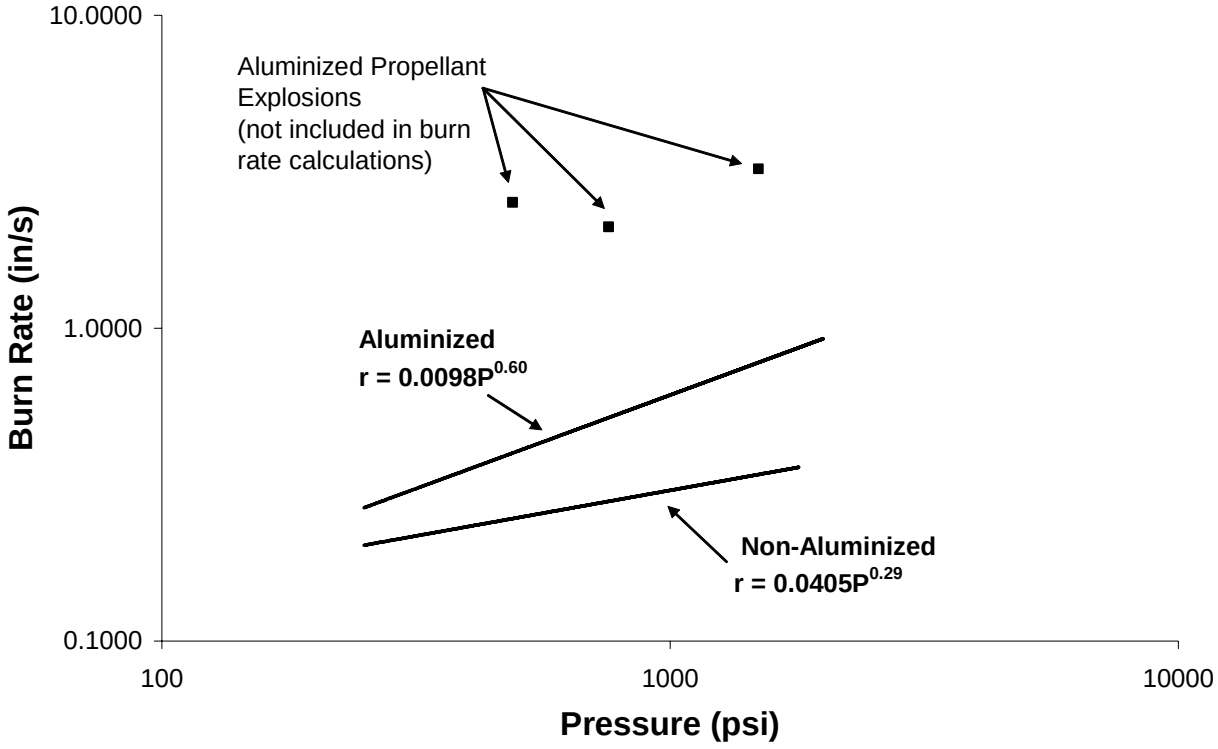

Figure 21: Burn Rate Comparison of Baseline Propellants - Al/AP/HTPB vs. AP/HTPB

By inspection, the aluminized propellant's burn rate is higher at all pressures between 250psi and 2000psi. (Fig. 21) By extrapolating each burn rate curve, the burn rate of the aluminized propellant would be expected to be greater for all pressures above 100psi.

Several interesting features become apparent through comparing the emission spectra from both propellants, shown in Figure 22. The top two curves are spectral data from aluminized baseline propellant. The bottom two curves are representative of the baseline AP/HTPB propellants. While in each plot, blackbody radiation appears to be interfering with the resolution, there appears to be an increase in emission near the 520nm region. The blue-green AlO emission bands occur from 430nm to 550nm (Ye et al., 1988). The increased emission is

due to the aluminum combusting. One of the first stages of aluminum's oxidation process is AlO production. Although short in duration, AlO identification validates the notion that the aluminum powder is combusting in the propellant. The final state of combusted aluminum is Al_2O_3.

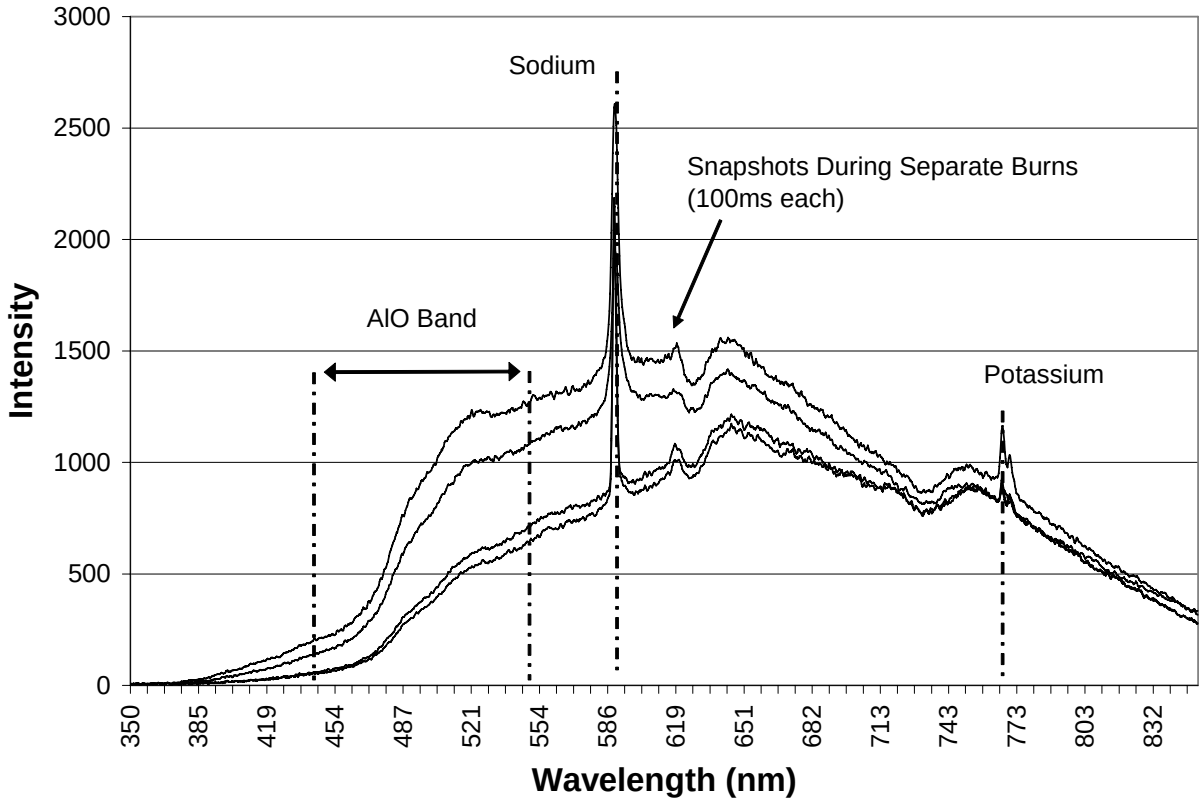

Figure 22: Al/AP/HTPB vs. AP/HTPB Baseline Propellants

The reaction zone temperature can be approximated by comparing the overall intensity curve to the blackbody intensity curve defined by the Planck distribution at a given temperature (Incropera and DeWitt, 2002). The Planck distribution is given by:

$$I_{\lambda,b}(\lambda,T) = \frac{2hc_0^2}{\lambda^5\left[\exp\left(\frac{hc_0}{\lambda kT}\right)-1\right]}$$

where:

$$h = 6.6256\times10^{-34}\, J\cdot s$$

$$k = 1.3805\times10^{-23}\,\frac{J}{K}$$

$$c_0 = 2.998\times10^{8}\,\frac{m}{s}$$

The Planck distribution shows the relative intensity as a function of wavelength (in μm) and temperature.

AP/HTPB Baseline Propellant: Time-Dependent Study

The USB2000's ability to record data in sequential segments of time helps researchers to identify changing combustion products during the burning process. Figure 23 outlines the course of a propellant test. Starting from ignition, the intensity grows over a period of 1.3 seconds, then begins to decrease until extinction at 3.1 seconds. Several features become evident from developing a time-resolved emission spectra plot. The primary feature is the appearance of sodium from the moment of ignition throughout the burn. The second event is the appearance of potassium. At ignition this emission is not seen. First apparent at t=0.2 seconds, the emission remains through the t=1.3 second peak emission. By t=1.5 seconds, the peak disappears and does not return.

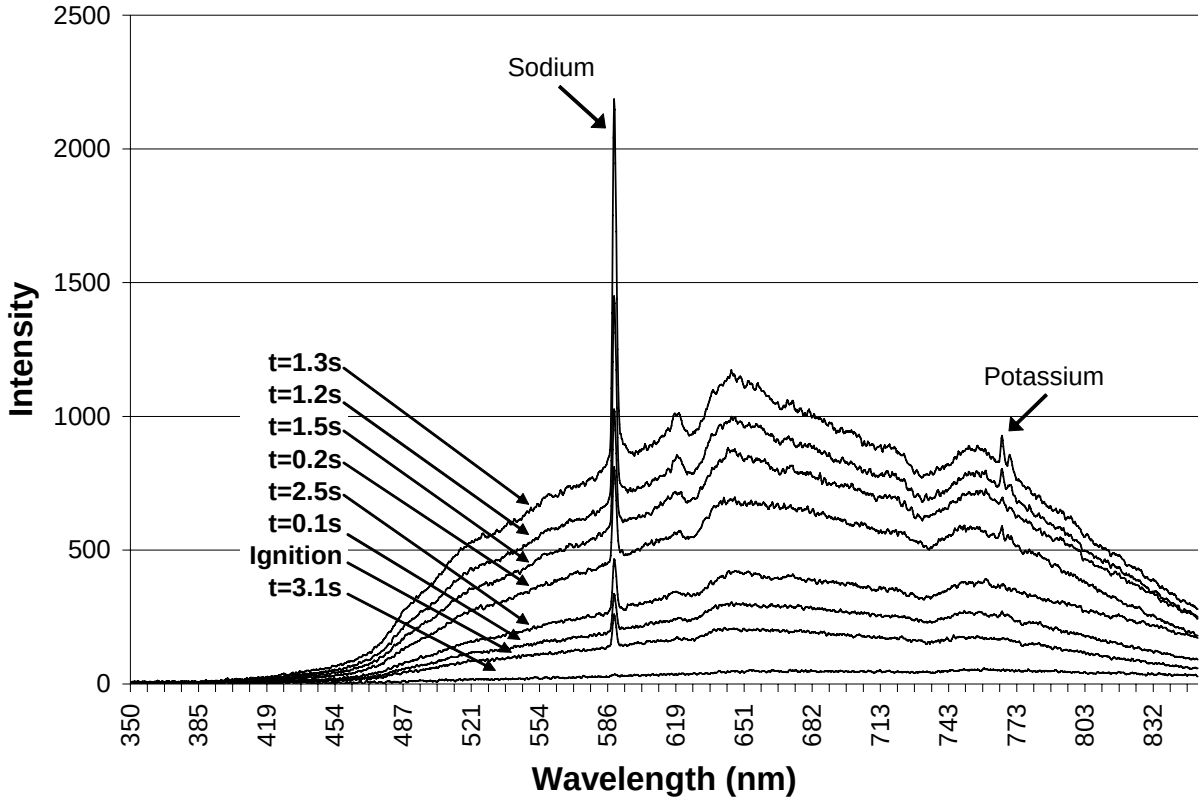

Figure 23: Time-Resolved Spectra for AP/HTPB Baseline Propellant

Spectral Identification of an Explosion

Occasionally the propellant strand will begin to combust at a much higher rate than expected. A premature explosion occurs; most likely the result of combustion gases propagating through voids and cracks in the propellant. This happens when the side of the strand ignites or when the burning end encounters an air pocket embedded within the propellant. Each of the diagnostics clearly identifies an explosion.

One such event occurred in the baseline Al/AP/HTPB propellant tested in the current experiment. The sample was to be tested at 1500psi. Data collected from the photodiode and pressure transducer are shown in Figure 24.

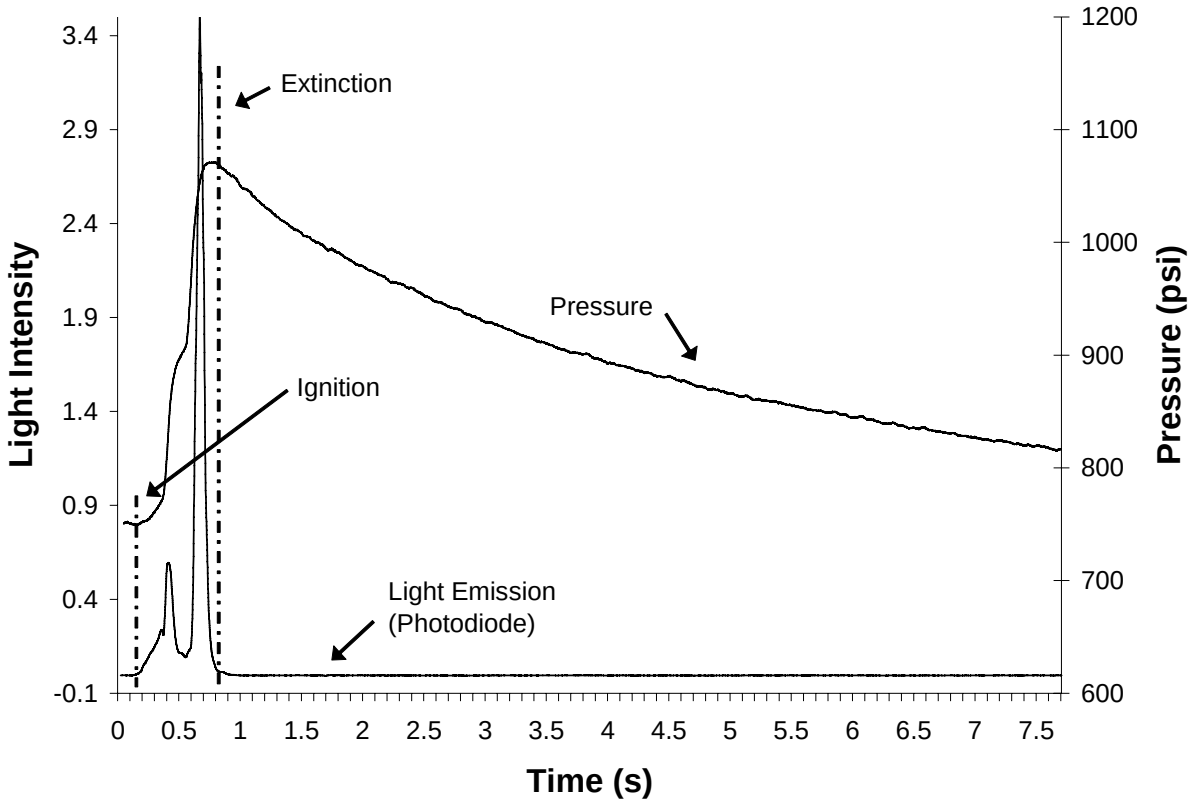

Figure 24: Pressure and Light Emission - Al/AP/HTPB Baseline Explosion

The sample was measured at 0.75", and a burn rate of 0.9-1.0 in/s was expected. This sample instead measured a burn rate of 3.23 in/s, over three times the appropriate burn rate for this propellant combination. A closer look at the burning region identifies more detail of the burn. (Fig. 25)

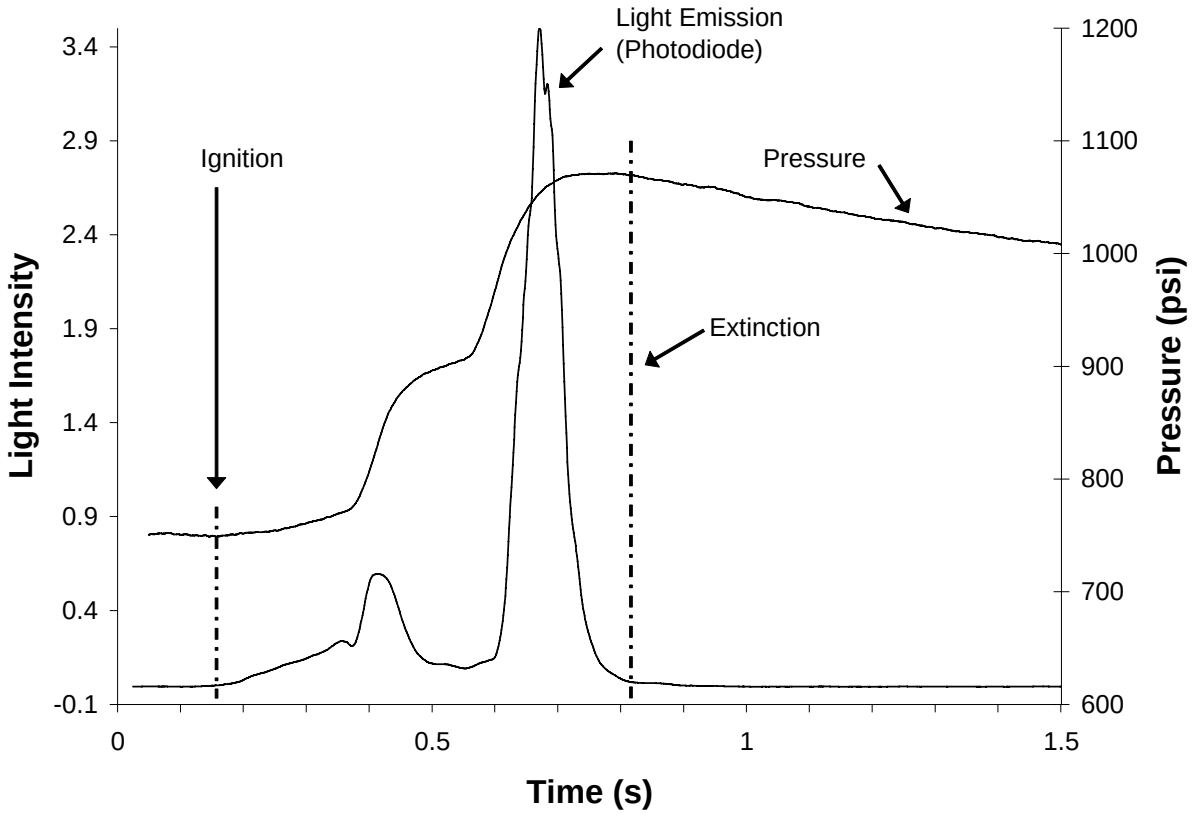

Figure 25: Pressure and Light Emission - Al/AP/HTPB Baseline Explosion - Detailed View

The point of ignition occurs at 0.15s, where both the pressure and light data begin to increase. The pressure increases are not steady, as expected, but rather show a sequence of two rapid increases before burning out. The light emission data shows two significant peaks of intensity that correspond to the sudden rises in pressure. The small propellant sample exploded in two short bursts.

The spectrometer data agree with the sudden increase in light output.

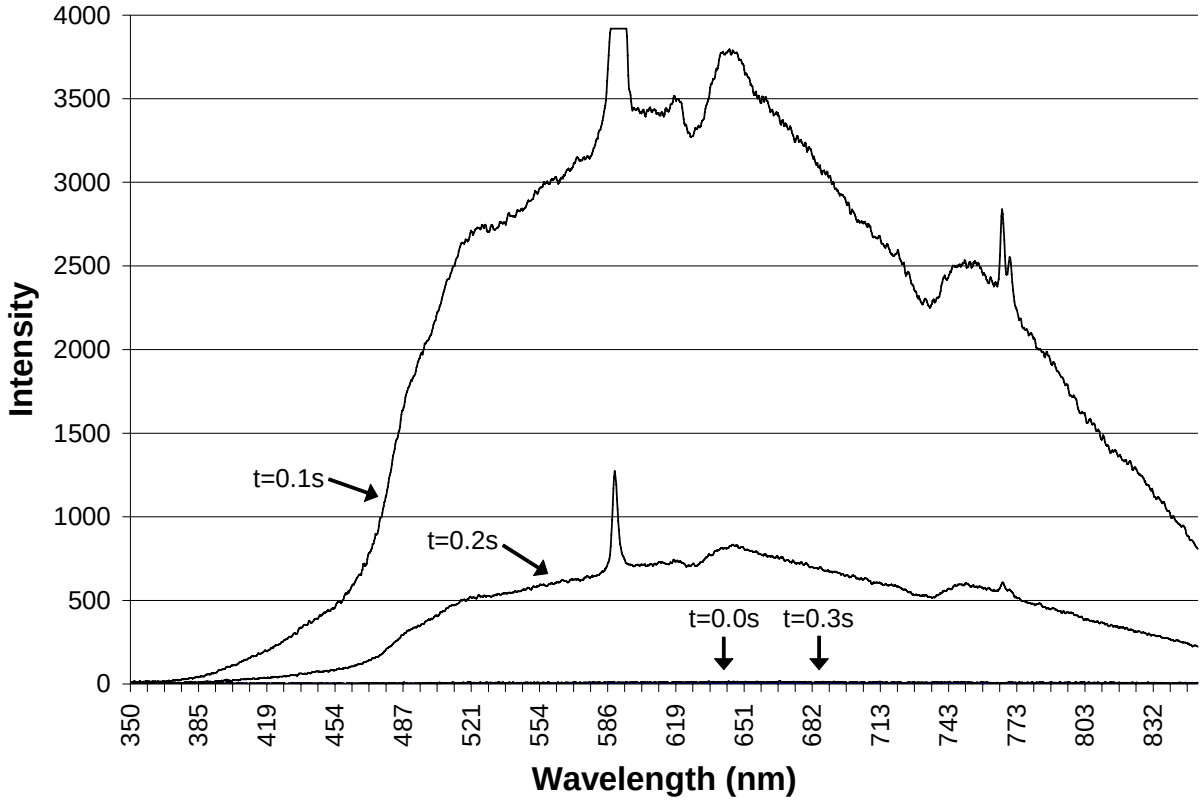

Figure 26: Time Resolved Plot of Propellant Explosion, Al/AP/HTPB Baseline Mixture

Figure 26 shows less than a half second in time. At t=0, the spectrometer was recording no light emission. One-tenth of a second later, the spectrometer was registering a maximum input at the 589nm wavelength and the intensity level across the measured spectrum was higher than the nominal input intensity. One-tenth of a second later, the intensity has settled down. Finally, after three-tenths of a second the sample has finished combusting. Both the rapid burn time as well as the higher-than-normal spectral intensity corroborates the pressure transducer and photodiode data. The exploding sample presents a unique data set that easily separates itself from the samples that combusted properly.

CHAPTER FIVE: CONCLUSIONS AND RECOMMENDATIONS

Conclusions

The initial data collected through the incorporation of a spectroscopy diagnostic appear to provide valuable information, complementing the existing pressure and broadband light emission data. During experimentation, the collected data provide solid rocket propellant researchers information detailing the presence of combusting ingredients, or lack thereof. The new diagnostic supports the existing data collection methods by further confirming the identification of a premature explosion.

The strong emission from AlO that was expected did not present itself as clearly as desired above the background thermal emission from particles and within the 1-nm resolution of the spectrometer, yet the data still support existence of aluminum combustion in the appropriate fuels. The comparisons of aluminized and non-aluminized propellants clearly demonstrate the differences. From an emission perspective, the diagnostic verified the similarity of baseline and bimodal AP propellants. The burn rate data, however, showed a clear difference.

Both variations of non-aluminized propellant demonstrated increased stability over the aluminized counterpart. This feature is noted by comparing the pressure exponents from each propellant's burn rate equation. The aluminized propellant possessed an exponent of 0.60 where the non-aluminized propellants demonstrated exponents of 0.29 (baseline) and 0.47 (bimodal).

The strong appearance of sodium in the spectroscopy data may lend itself to further analysis. The relative strength of this feature as compared to the other spectral data might permit a detailed study of the shape and width of the feature, allowing further insight and understanding

of the combustion occurring within the strand burner. The sodium spike is shown to be highly visible across all pressure ranges.

The spectrometer has effectively identified and validated the existence of a premature explosion during a sample. Being able to properly identify and reject these samples is vital to collecting and analyzing accurate and repeatable data.

Recommendations

Several recommendations have surfaced through the initial integration and testing of the spectroscopy diagnostic. These recommendations primarily exist as a means of improving the current configuration.

The spectrometer presently employed possesses a resolution of approximately 1 nm. A spectrometer with a higher resolution will be better able to distinguish unique spectral features that would otherwise not be identified. In a similar effort to increase resolution and precision, the application of optical filters, other than Neutral Density, to isolate spectral bands of interest or eliminate unwanted emissions will assist in identifying hard to locate emissions.

Other potential ideas for future incorporation include expanding the test pressure range. The strand burner facility at The University of Central Florida is capable successful tests at pressures up to around 5000 psi. The current effort explored up to 2000 psi. The optical emission from solid rocket propellants may begin to vary as pressures become higher.

With the increased interest in additives to traditional solid rocket propellants, an emission spectroscopy diagnostic will aid in identifying and validating the combustion of the new components. Showing the change in burn rate data could be paralleled with spectroscopy data

confirming the new ingredient's combustion within the propellant, thus validating the notion that the new chemical did indeed affect the solid propellant characteristics.

Finally, a new strand burner incorporating optical ports on opposite sides of the burner will allow more advanced spectroscopy experiments, beyond the emission based diagnostic. In the future, even laser-based diagnostics could be incorporated to further advance the understanding of the complex combustion chemistry contained within composite solid propellants.

APPENDIX A: SPECTROMETER CALIBRATION SHEET

OOIBASE32

Ocean Optics Inc.
First in Photonics™

Wavelength Calibration Data Sheet

Ocean Optics, Corp.

Built For:	**Siemens Westinghouse**
Order Number:	**23242**
Model:	**USB2000**
Description:	Fiber Optic Spectrometer
Grating:	600 Lines Blazed at 300 nm
Bandwidth:	200 - 850 nm
Options Installed:	OFLV-2 Detector, 25um Slit
Serial Number:	**USB2E471** **Master**

λ	Pixel #	Predicted λ	Δλ
253.652	180	253.607	0.045
296.728	301	296.664	0.064
302.150	317	302.326	-0.176
334.148	407	334.032	0.116
365.015	496	365.141	-0.126
404.656	610	404.622	0.034
407.781	619	407.720	0.061
435.835	701	435.828	0.007
546.074	1030	546.204	-0.130
576.959	1124	576.993	-0.034
579.065	1130	578.947	0.118
696.543	1500	696.527	0.016
706.722	1533	706.727	-0.005
727.294	1600	727.285	0.009
738.398	1637	738.549	-0.151
750.900	1676	750.354	0.546
763.510	1720	763.587	-0.077
772.421	1750	772.556	-0.135
794.817	1825	794.791	0.026
800.616	1846	800.968	-0.352
811.531	1882	811.507	0.024
826.452	1934	826.616	-0.164
842.160	1987	841.876	0.284

Calibration Coefficients

First Coefficient:	0.362323425
Second Coefficient:	-1.26959E-05
Third Coefficient:	-2.13486E-09
Intercept:	188.8129609
Regression Fit:	0.999999243

Stray Light Measurements (AU)

Holmium Oxide (444nm):	1.20
Yellow Dye:	2.13
Blue Dye:	3.01
Molybdate:	1.73
OG550 Filter:	2.51
RG850 Filter:	4.00
FG3 Filter:	1.17

11/17/00

APPENDIX B: FIBER OPTIC CABLE CALIBRATION SHEET

Ocean Optics Inc.
First in Photonics

Fiber Assembly Report

Item Code

P50-2-VIS/NIR

Date:	**September 19, 2005**
Lot #:	EOS00634-12
Connector 1 #:	SMA-905
Connector 2 #:	SMA-905

www.OceanOptics.com
Phone:727-733-2447
Fax:727-733-3962
Info@OceanOptics.com
830 Douglas Ave.
Dunedin, FL 34698

Home of the **"BEST FOR SPECTROSCOPY"** brand of Optical Fiber

Ask about our custom line of Optical Probes and Assemblies

Fiber Lot #:	FB-398-2-1	**Fiber Buffer Material:**	Polyimide
Fiber Type:	Low OH	**Epoxy Used:**	Epotek 353
Clad/Core Ratio:	1:2.4	**Jacketing:**	Blue Zip Tube
Numerical Aperature:	.22	**Length (meters):**	2.00
Fiber Core Diameter:	50um		

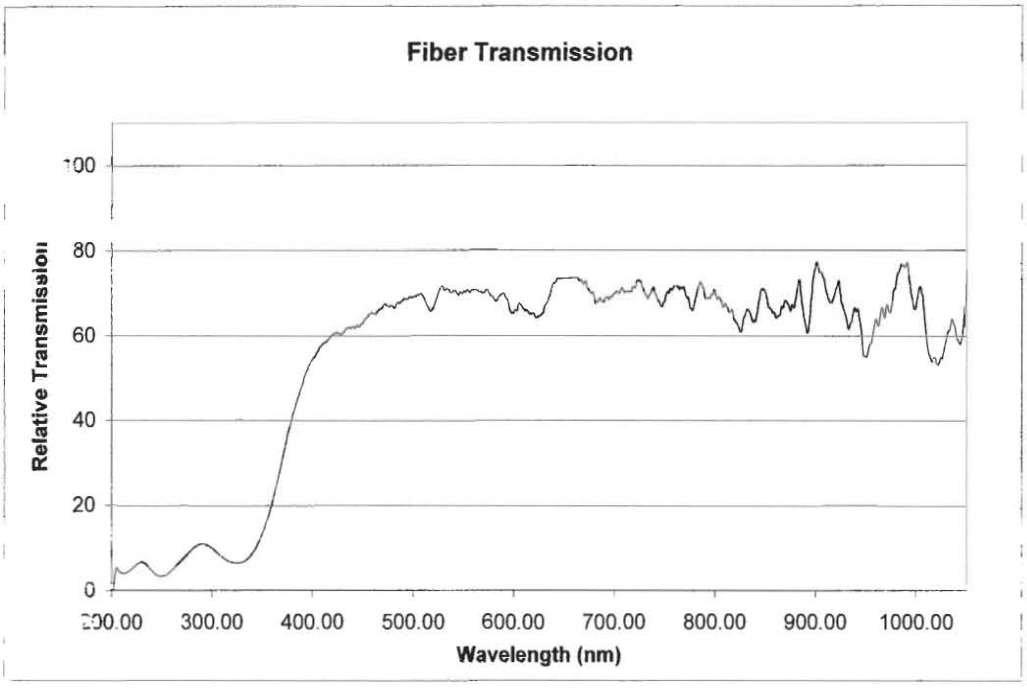

Inspection Checklist

Polish: ✓
Concentricity: ✓
Cap Placement: ✓
Labeling: ✓
Color Coding: ✓
Ferrule length: ✓

Inspected by: Ruby Fenton

APPENDIX C: SPECTROMETER DATA SHEET (PARTIAL)

830 Douglas Ave.
Dunedin, FL 34698
(727)733-2447
Fax:(727)733-3962
www.OceanOptics.com

Ocean Optics Inc.
First in Photonics™

A HALMA GROUP COMPANY

USB2000 Data Sheet

Description

The Ocean Optics USB2000 Spectrometer includes the linear CCD-array optical bench, plus all the circuits necessary for spectrometer operation. The result is a compact, flexible system, with no moving parts, that's easily integrated as an OEM component.

The USB2000 spectrometer is a unique combination of technologies providing users with both an unusually high spectral response and good optical resolution in a single package. The electronics have been designed for considerable flexibility in connecting to various USB2000 series modules as well as external interfaces. The USB2000 interfaces to PCs, PLCs and other embedded controllers through wither USB or RS-232 communications. The information included in this guide provides detailed instructions on the connection and operation of the USB2000.

The detector used in the USB2000 spectrometer is a high-sensitivity 2048-element CCD array from Sony, product number ILX511. (For complete details on this detector, visit Sony's web site at www.sony.com. Ocean Optics applies a coating to all ILX511 detectors, so the optical sensitivity could vary from that specified in the Sony datasheet)

The USB2000 operates off of a single +5VDC supply and either a USB or RS-232 interface. The USB2000 is a microcontroller-controlled spectrometer, thus all operating parameters are implemented through software interfacing to the unit.

The USB2000 has a 10 pin external interface to easily integrate with Ocean Optics other modular components to for an entire system.

Features

- High sensitivity of up to 90 photons/counts
- An optical resolution of ~0.3nm (FWHM)
- A wide variety of optics available
  - 14 gratings
  - 6 slit widths
  - 3 detector coatings
  - 6 optical filters
- Integration times from 3 to >30000 ms
- Embedded microcontroller allows programmatic control of all operating parameters
- EEPROM storage for
  - Wavelength Calibration Coefficients
  - Linearity Correction Coefficients
  - Other Configuration Parameters
- Low power of only 450 mW
- 12 bit, 1MHz A/D Converter
- 3 triggering modes
- 2 strobe signals for triggering other devices
- Programmable for Standalone Operation
- Plug-n-Play Interface for PC applications
- CE Certification

Specifications

Specifications	Criteria
Absolute Maximum Ratings:	
V_{CC}	+ 5.5 VDC
Voltage on any pin	Vcc + 0.2 VDC
Physical Specifications:	
Physical Dimensions	90 mm x 65 mm x 35 mm
Weight	190 g
Power:	
Power requirement (master)	95 mA at +5 VDC
Supply voltage	4.5 – 5.5 V
Power-up time	~5s depending on code size
Spectrometer:	
Design	Asymmetric crossed Czerny-Turner
Focal length (input)	42mm
Focal length (output)	68mm (75, 83, and 90mm focal lengths are also available)
Input Fiber Connector	SMA 905
Gratings	14 different gratings
Entrance Slit	5, 10, 25, 50, 100, or 200 µm slits. (Slits are optional. In the absence of a slit, the fiber acts as the entrance slit.)
Detector	Sony ILX511 CCD
Filters	2nd and 3rd order rejection, long pass (optional)
Spectroscopic:	
Integration Time	3 – >30,000 msec
Dynamic Range	2×10^8
Signal-to-Noise	250:1 single acquisition
Readout Noise (single dark spectrum)	3.5 counts RMS, 20 counts peak-to-peak
Resolution (FWHM)	0.03 – 10.0 nm varies by configuration (see www.Oceanoptics.com for configuration options)
Stray Light	<0.05% at 600 nm; <0.10% at 435 nm
Spectrometer Channels	One
Environmental Conditions:	
Temperature	-30° to +70° C Storage & -10° to +50° C Operation
Humidity	0% - 90% noncondensing
Interfaces:	
USB	USB 1.1, 12 Mbps
RS-232	2-wire RS-232

Mechanical Diagrams

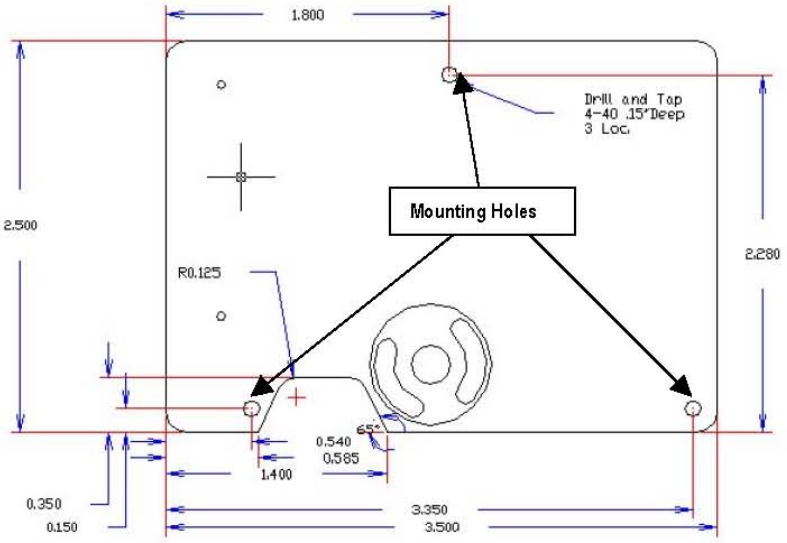

Figure 1: USB2000 Outer Dimensions (Bottom View)

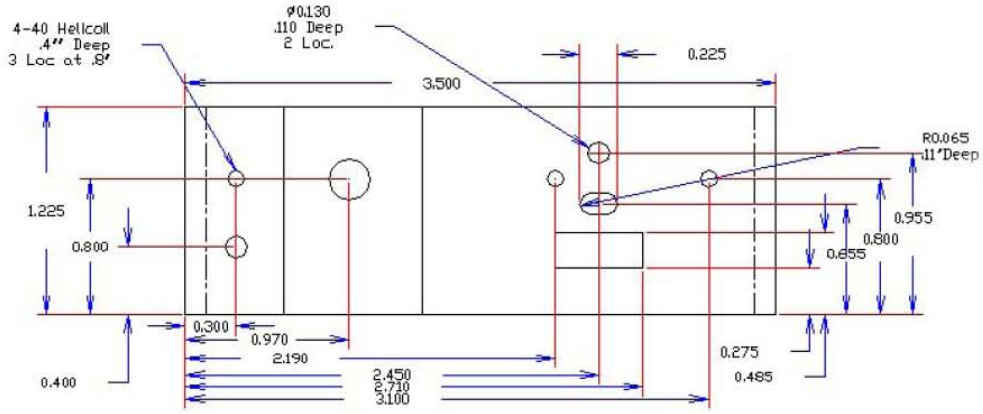

Figure 2: USB2000 Outer Dimensions (Inverted Front View)

APPENDIX D: MATHCAD STRAND BURNER MODEL

Input Variables:

$P_i := 5000psi$ <= Initial Pressure

$T_{init} := 30$ <= Initial Temperature (in Celsius)

$d_{SB} := 3.1in$ <= Diameter of the Strand Burner

$L_{SB} := 9.0in$ <= Length of the Strand Burner

Propellant Details

$r := .87\frac{in}{s}$ <= Burn Rate of Propellant

$L_{strand} := .952in$ <= Length of the Propellant Strand

$T_{AF} := 2500K$ <= Adiabatic flame temperature of propellant

$d_{strand} := .25in$ <= Diameter of the Propellant Strand

$\rho_{prop} := 1.82\frac{gm}{cm^3}$ <= Density of the Propellant Strand

Initial Calculations

$kJ \equiv 1000J$

$kPa \equiv 1000Pa$

$R_u := 8314.3\frac{J}{kg \cdot mol \cdot K}$

$T_i := (T_{init} + 273.15)K$

$V_{SB} := \pi\frac{d_{SB}^2 \cdot L_{SB}}{4}$ $V_{SB} = 1113\,cm^3$

$A_{prop} := \pi\frac{d_{strand}^2}{4}$ $A_{prop} = 0.317\,cm^2$

$m_{dot\_in} := r \cdot A_{prop} \cdot \rho_{prop}$ $m_{dot\_in} = 1.274 \times 10^{-3}\frac{kg}{s}$

$\frac{L_{strand}}{r} = 1.094\,s$

$A_{prop} \cdot \rho_{prop} \cdot L_{strand} = 1.394\,gm$

$C_{p\_prop} := C_{pAr}$

Argon Details

$MM_{Ar} := \frac{39.948}{mol}$

$R_{Ar} := 0.2081\frac{kJ}{kg \cdot K}$

$C_{pAr} := 0.519\frac{kJ}{kg \cdot K}$

$\gamma_{Ar} := 1.67$

$\rho_{Ar} := \frac{P_i}{\left(\frac{R_u}{MM_{Ar}} \cdot T_i\right)}$ $\rho_{Ar} = 546.388\frac{kg}{m^3}$

$m_{Ar} := \frac{(P_i \cdot V_{SB} \cdot MM_{Ar})}{R_u \cdot T_i}$ $m_{Ar} = 0.608\,kg$

Index Counters

$$i := 0 .. \frac{1000 \cdot L_{strand}}{r \cdot s} \qquad j := \left(\frac{L_{strand}}{r \cdot s} \right) \cdot 1000 .. 3000$$

Pressure Calculations

$$\Delta T_i := \gamma_{Ar} \cdot T_{AF} \cdot \frac{m_{dot\_in}}{m_{Ar}} \cdot \frac{i}{1000} \cdot s$$

$$P1_i := \left[\frac{\left[\left(m_{dot\_in} \cdot \frac{i \cdot s}{1000} \right) + m_{Ar} \right]}{V_{SB}} \right] \cdot \left(\frac{R_u}{MM_{Ar}} \right) \cdot \left(T_i + \Delta T_i \right)$$

$$P_i := P1_i \quad end := rows\left(P_1\right) - 1 \quad j := end .. 3000 \quad k := 0 .. 3000$$

$$P_2 := \left[\frac{\left[\left(m_{dot\_in} \frac{L_{strand}}{r} \right) + m_{Ar} \right]}{V_{SB}} \right] \cdot \left(\frac{R_u}{MM_{Ar}} \right) \cdot \left(T_i + \Delta T_{end} \right) \quad P_j := P_2$$

$$P1b_i := \left[\frac{\left[\left(s \cdot m_{dot\_in} \cdot \frac{i}{1000} \right) + m_{Ar} \right]}{V_{SB}} \right] \cdot \left(\frac{R_u}{MM_{Ar}} \right) \cdot T_i$$

$$P_{b_i} := P1b_i \quad end_b := rows\left(P_{1b}\right) - 1 \quad j_b := end_b .. 3000 \quad k_b := 0 .. 3000$$

$$P_{2b} := \left[\frac{\left[\left(m_{dot\_in} \frac{L_{strand}}{r} \right) + m_{Ar} \right]}{V_{SB}} \right] \cdot \left(\frac{R_u}{MM_{Ar}} \right) \cdot T_i \quad P_{b_j} := P_{2b}$$

Pressure Increase Due to Energy:

$P_2 - P_{2b} = 158.119\,psi$

Final Pressure after Thermodynamic Equilibrium:

$P_{2b} = 5011.458\,psi$

Maximum Pressure Reached During Burn:

$P_2 = 5169.577\,psi$

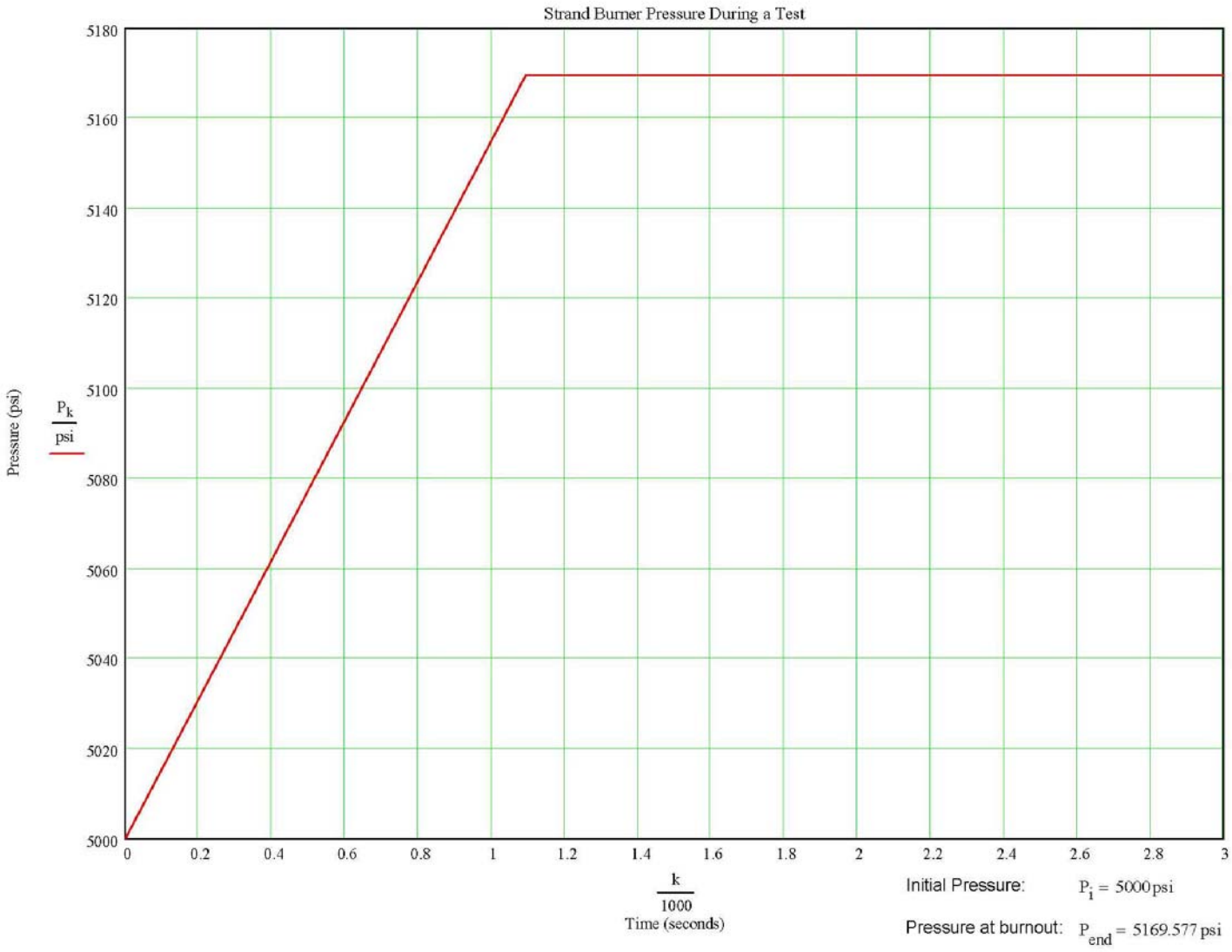
Strand Burner Pressure During a Test
Pressure (psi)
P_k / psi
5180
5160
5140
5120
5100
5080
5060
5040
5020
5000
0
0.2
0.4
0.6
0.8
1
1.2
1.4
1.6
1.8
2
2.2
2.4
2.6
2.8
3
k / 1000
Time (seconds)
Initial Pressure: $P_i = 5000\,psi$
Pressure at burnout: $P_{end} = 5169.577\,psi$

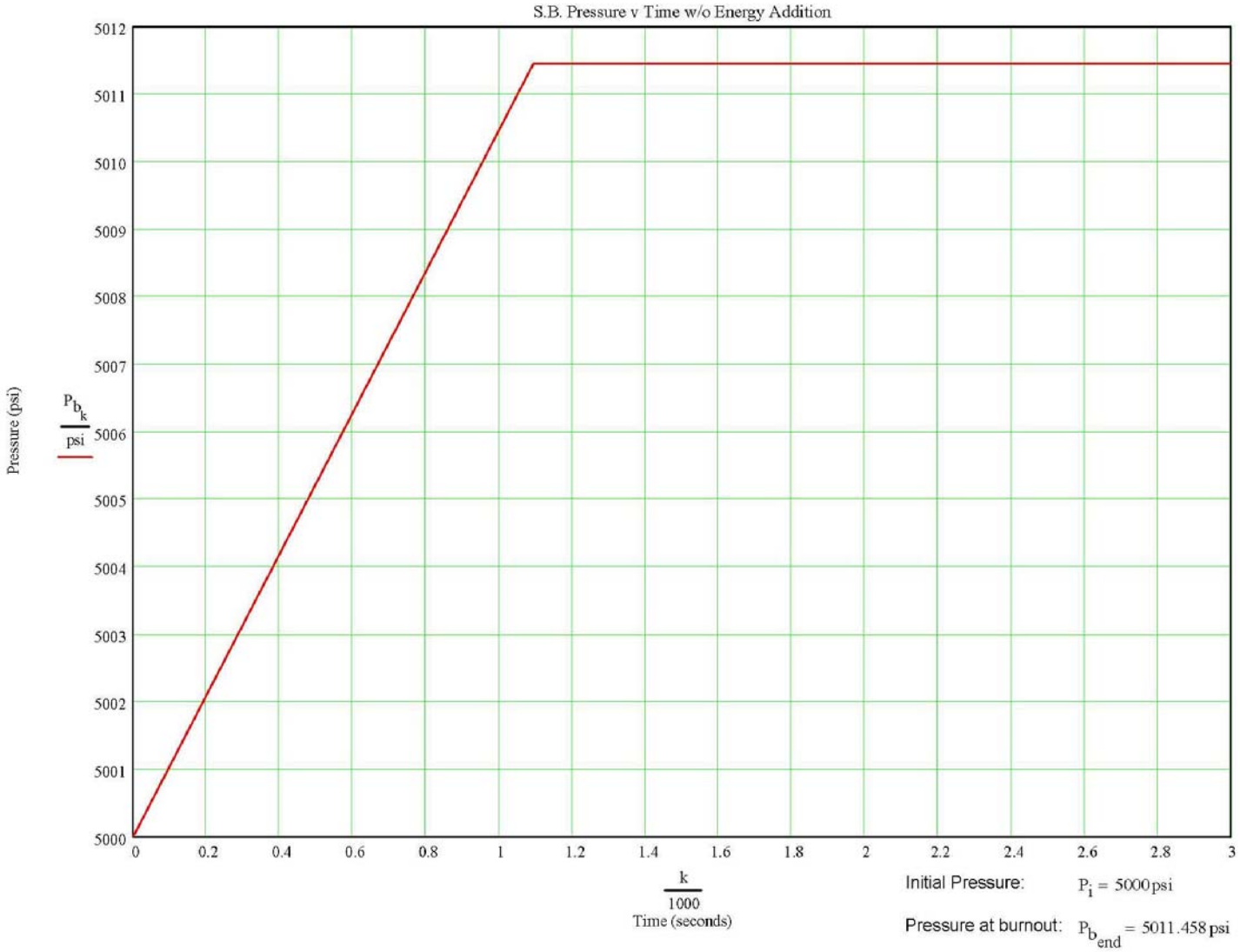
S.B. Pressure v Time w/o Energy Addition
Pressure (psi)
P_{b_k} / psi
5012
5011
5010
5009
5008
5007
5006
5005
5004
5003
5002
5001
5000
0
0.2
0.4
0.6
0.8
1
1.2
1.4
1.6
1.8
2
2.2
2.4
2.6
2.8
3
k / 1000
Time (seconds)
Initial Pressure: $P_i = 5000\,psi$
Pressure at burnout: $P_{b_{end}} = 5011.458\,psi$

LIST OF REFERENCES

Apte, S., Yang, V. (2002) "Unsteady Flow Evolution and Combustion Dynamics of Homogeneous Solid Propellant in a Rocket Motor," *Combustion and Flame*, Vol. 131, pp. 110-131.

Arvanetes, J., Petersen, E.L. (2006) "Monitoring Strand Burner Combustion Products Using Emission Spectroscopy," AIAA Paper 2006-5251.

Arvanetes, J., Stephens, M., Carro, R., Powell, A., Wolf, S., Petersen, E.L., Smith, C., Whittinghill, G. (2005) "Burn Rate Measurements of AP-Based Composite Propellants at Elevated Pressures," Proceedings of the 4th Joint Meeting of the U.S. Sections of The Combustion Institute.

Blomshield, F. S., Nguyen, S., Matheke, H., Atwood, A., and Bui, T. (2004) "Acoustic Particle Damping of Propellants Containing Ultra-Fine Aluminum," AIAA Paper 2004-3722.

Brill, T. B. and Budenz, B. T., "Flash Pyrolysis of Ammonium Percholrate-Hydroxyl-Terminated-Polybutadiene Mixtures Including Selected Additives," *Solid Propellant Chemistry, Combustion, and Motor Interior Ballistics*, Vol. 185, Progress in Astronautics and Aeronautics, Yang, V., Brill, T., and Ren, W.Z. (Ed.), AIAA, Reston, VA, 2000, pp. 3-32.

Brousseau, P., Anderson, C.J. (2002) "Nanometric Aluminum in Explosives," *Propellants, Explosives, Pyrotechnics*, Vol. 27, No. 5, pp. 300-306.

Bukaemskii, A. A. (2002) "Physical Model of Explosive Synthesis of Ultrafine Aluminum Oxide," *Combustion, Explosion, and Shock Waves*, Vol. 38, No. 3, pp. 360-364.

Carro, R., Arvanetes, J., Powell, A., Stephens, M., Petersen, E., and Smith, C. (2005) "High-Pressure Testing of Composite Solid Propellant Mixtures: Burner Facility Characterization," AIAA Paper 2005-3617.

Chakravarthy, S. R., Seitzman, J. M., Lillard, R., Price, E. W., and Sigman, R. K. (2001) "Intermittent Burning and its Contribution to Plateau Burning of Composite Propellants," AIAA Paper 2001-0339.

Davenas, A., "Development of Modern Solid Propellants," *Journal of Propulsion and Power*, Vol. 19, No.6, 2003, pp. 1108-1128.

DeLuca L.T., Galfetti, L., Severini, F., Meda, L., Marra, G., Vorozhtsov, A.B., Sedoi, V.S., Babuk, V.A. (2005) "Burning of Nano-Aluminized Composite Rocket Propellants," *Combustion, Explosion, and Shock Waves*, Vol. 41, No. 6, pp. 680-692.

Dokhan, A., Price, E. W., Seitzman, J. M., and Sigman, R. K. (2002a) "Combustion Mechanisms of Bimodal and Ultra-Fine Aluminum in AP Solid Propellant," AIAA Paper 2002-4173.

Dokhan, A., Price, E. W., Seitzman, J. M., and Sigman, R. K. (2002b) "The Effects of Bimodal Aluminum with Ultrafine Aluminum on the Burning Rates of Solid Propellants," *Proceedings of the Combustion Institute*, Vol. 29, pp. 2939-2945.

Dokhan, A., Price, E. W., Seitzman, J. M., and Sigman, R. K. (2003) "The Ignition of Ultra-Fine Aluminum in Ammonium Perchlorate Solid Propellant Flames," AIAA Paper 2003-4810.

Dokhan, A., Price, E. W., Sigman, R. K., and Seitzman, J. M. (2001) "The Effects of Al Particle Size on the Burning Rate and Residual Oxide in Aluminized Propellants," AIAA Paper 2001-3581.

Evans, B., Favorito, N. A., Boyer, E., Risha, G. A., Wehrman, R. B., and Kuo, K. K. (2004) "Characterization of Nano-Sized Energetic Particle Enhancement of Solid-Fuel Burning Rates in an X-Ray Transparent Hybrid Rocket Engine," AIAA Paper 2004-3821.

Fedorov, A.V., Kharlamova, Y.V. (2003) "Ignition of an Aluminum Particle," *Combustion, Explosion, and Shock Waves*, Vol. 39, No. 5, pp. 544-547.

Fitzgerald, R. P. and Brewster, M. Q. (2004) "Flame and Surface Structure of Laminate Propellants with Coarse and Fine Ammonium Perchlorate," *Combustion and Flame*, Vol. 136, pp. 313-326.

George, P., Krishnan, S., Varkey, P.M., Ravindran, M., Ramachandran, L. (2001) "Fuel Regression Rate in Hydroxyl-Terminated-Polybutadine/Gaseous-Oxygen Hybrid Rocket Motors," *Journal of Propulsion and Power*, Vol. 17, No. 1, pp. 35-42.

Glotov, O.G. (2002) "Condensed Combustion Products of Aluminized Propellants. III. Effect of an Inert Gaseous Combustion Environment," *Combustion, Explosion, and Shock Waves*, Vol. 38, No. 1, pp. 92-100.

Glumac, N., Krier, H., Bazyn, T., Eyer, R. (2005) "Temperature Measurements of Aluminum Particles Burning in Carbon Dioxide," *Combustion Science and Technology*, Vol. 177, pp. 485-511.

Granier, J. J. and Pantoya, M. L. (2004) "Laser Ignition of Nanocomposite Thermites," *Combustion and Flame*, 138, pp. 373-383.

Herzberg, G. Molecular Spectra and Molecular Structure, Vol. 1, Krieger Pub Co, Malabar, 1950.

Hudson, M.K., Shanks, R.B., Snider, D.H., Lindquist, D.M., Luchini, C., Rooke, S. (1998) "UV, Visible, and Infrared Spectral Emissions in Hybrid Rocket Plumes," International Journal of Turbo and Jet Engines, Vol. 15, pp. 71-87

Incropera, F.P., DeWitt, D.P., Introduction to Heat Transfer, 4th ed., John Wiley and Sons, New York, NY, 2002.

Lessard, P., Beaupré, F., and Brousseau, P. (2001) "Burn Rate Studies of Composite Propellants Containing Ultra-Fine Metals," *Energetic Materials - Ignition, combustion and detonation,* Karlsruhe, Germany; 3-6 July, pp. 88.1-13.

Lide, D.R., Ed., CRC Handbook of Chemistry and Physics, 83rd ed., CRC Press, Boca Raton, FL, 2002.

Linton, C., Nicholls, R.W. (1969) "Relative Band Strengths for the AlO Blue-Green System," *Journal of Quantative Spectroscopy and Radiative Transfer*, Vol. 9, pp. 1-11.

Lou, R.L., Katzakian, A. (1971) "Fast-Burning Rate/High Slope Propellant Technology Program Final Report," U.S. Navy Report, Naval Weapons Center, China Lake, CA.

Mamen, J., Goroshin, S., Higgins, A. (2005) "Spectral Structure of the Aluminum Dust Flame," 20th International Colloquium on the Dynamics of Explosions and Reactive Systems.

Maxwell, K.L., Hudson, M.K. (2005) "Spectral Study of Molecular Bands in Hybrid Rocket Plumes," *Journal of Pyrotechnics*, Issue 21, pp. 59-69.

Mench, M. M., Yeh, C. L., Kuo, K. K. (1998) "Propellant Burning Rate Enhancement and Thermal Behavior of Ultra-Fine Aluminum Powders (Alex)," Proceedings of the 29th Annual Conference of ICT, pp. 30-1–30-15.

Parr, T., Hanson-Parr, D., "Optical Diagnostics of Solid-Propellant Flame Structures," *Solid Propellant Chemistry, Combustion, and Motor Interior Ballistics*, Vol. 185, Progress in Astronautics and Aeronautics, Yang, V., Brill, T., and Ren, W.Z. (Ed.), AIAA, Reston, VA, 2000, pp. 381-411.

Popenko, E.M., Il'in, A.P., Gromov, A.M., Kondratyuk, S.K., Surgin, V.A., Gromov, A.A. (2002) "Combustion of Mixtures of Commercial Aluminum Powders and Ultrafine Aluminum Powders and Aluminum Oxide in Air," *Combustion, Explosion, and Shock Waves*, Vol. 38, No. 2, pp. 157-162.

Price, E. W. and Sigman, R. K. (2000) "Combustion of Aluminized Solid Propellants," *Solid Propellant Chemistry, Combustion, and Motor Interior Ballistics*, Vol. 185, *Progress in Astronautics and Aeronautics*, Yang, V., Brill, T., and Ren, W.-Z. (Ed.), AIAA, Reston, VA, pp. 663-687.

Risha, G. A., Ulas, A., Boyer, E., Kumar, S., and Kuo, K. K. (2001) "Combustion of HTPB-Based Solid Fuels Containing Nano-Sized Energetic Powder in a Hybrid Rocket Motor," AIAA Paper 2001-3535.

Sambamurthi, J. K., Price, E. W., and Sigman, R. K. (1984) "Aluminum Agglomeration in Solid-Propellant Combustion," *AIAA Journal*, Vol. 22, pp. 1132-1138.

Schick, H.L., Thermodynamics of Certain Refractory Compounds: Discussion of Theoretical Studies, Vol. 1, Academic Press, New York, NY, 1966.

Schick, H.L., Thermodynamics of Certain Refractory Compounds: Thermodynamic Tables, Bibliography, and Property File, Vol. 2, Academic Press, New York, NY, 1966.

Small, J.L., Stephens, M.A., Deshpande, S., Petersen, E.L., Seal, S. (2005) "Burn Rate Sensitization of Solid Propellants Using a Nano-Titania Additive," 20th International Colloquium on the Dynamics of Explosions and Reactive Systems.

Stephens, M., Carro, R., Wolf, S., Sammet, T., Petersen, E., and Smith, C. (2005a) "Performance of AP-Based Composite Propellant Containing Nanoscale Aluminum," AIAA Paper 2005-4470.

Stephens, M.A., Petersen, E.L. (2005b) "Burn Rate Measurements of Bimodal Ammonium Perchlorate in HTPB/Al Composite Rocket Propellant," AIAA Region II Student Conference.

Sultzmann, K.G.P. (1975) "Shock-Tube Measurements of the f-Number for the Fundamental Vibration-Rotation bands of AlO in the $X^2\Sigma^+$ Electronic Ground State," *Journal of Quantative Spectroscopy and Radiative Transfer*, Vol. 15, pp. 313-331.

Sutton, G. P. and Biblarz, O. (2001) *Rocket Propulsion Elements*, John Wiley, New York.

Weiser, V., Eisenreich, N. (2005) "Fast Emission Spectroscopy for a Better Understanding of Pyrotechnic Combustion Behavior," *Propellants, Explosives, Pyrotechnics*, Vol. 30, No. 1.

Wilson, E.W., Mackey, J.E., Keller, B.D., Goertzen, E.J., Clements, S.A., Rivenbark, C.D., Cox, C. (2005) "OH Emission Spectra of Hybrid Rocket Motors Using PMMA and HTPB," AIAA Paper 2005-3905.

Wright, A.B., Elsasser, J.E., Hudson, M.K., Wright, A.M. (2005) "Optical Studies of Combustion Chamber Flame in a Hybrid Rocket Motor," *Journal of Pyrotechnics*, Issue 21, pp. 21-30.

Yang, Y., Wang, S., Sun, Z., Dlott, D.D. (2005) "Near-Infrared and Visible Absorption Spectroscopy of Nano-Energetic Materials Containing Aluminum and Boron," *Propellants, Explosives, Pyrotechnics*, Vol. 30, No. 3.

Ye, X., Yongkang, C., Xiaoliang, Z., "An Experimental Study of AlO Blue-Green ($B2\Sigma^+ - X^2\Sigma^+$) Band System in a Shock-Tube," *Shock Tubes and Waves*, Proceedings of the Sixteenth International Symposium on Shock Tubes and Waves, Grönig, H. (Ed.), Weinheim, Germany, 1988, pp. 511-516.